A 25-METER TELESCOPE for MILLIMETER WAVELENGTHS

SEPTEMBER, 1975

VOLUME I

NATIONAL RADIO ASTRONOMY OBSERVATORY

A 25-METER TELESCOPE FOR MILLIMETER WAVELENGTHS

September 1975

NATIONAL RADIO ASTRONOMY OBSERVATORY*
Charlottesville, Virginia

* Operated by Associated Universities, Inc., under contract with the National Science Foundation.

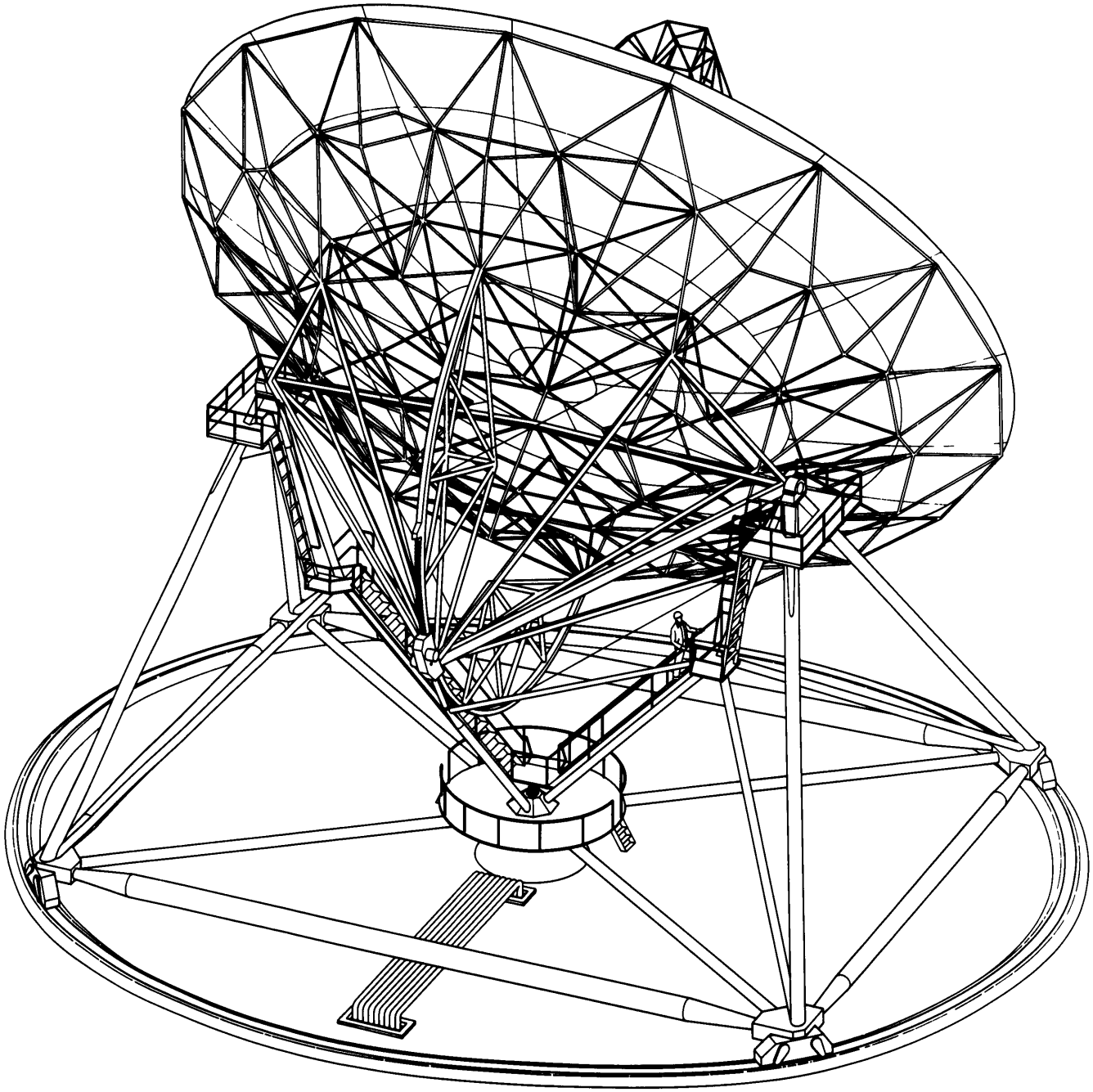

CONTENTS

FOREWARD

The work which is described in this report has been done by a group of scientists and engineers at the National Radio Astronomy Observatory. Members of this group, under the leadership of B. E. Turner, include W. R. Burns, J. W. Findlay, J. R. Fisher, M. A. Gordon, D. S. Heeschen, D. E. Hogg, W. G. Horne, H. Hvatum, K. I. Kellermann, L. J. King, H. S. Liszt, P. J. Napier, J. M. Payne, S. von Hoerner, C. M. Wade, S. Weinreb and W-Y. Wong.

The work has benefitted from discussions with a number of scientists from other institutions. In particular, L. E. Snyder (University of Virginia) contributed to Chapter II.

CHAPTER I

INTRODUCTION AND SUMMARY

A. INTRODUCTION

This is a report on the design of a 25-meter diameter telescope for use at millimeter wavelengths. With an rms surface error of 0.075 mm and a pointing accuracy of 1.2 arc seconds, the telescope will have good performance at wavelengths as short as 1.2 mm. At shorter wavelengths its efficiency will decline, but it should still be an extremely powerful instrument at wavelengths as short as 0.8 mm. While considerable design and development work remain to be done, the design is now far enough along to demonstrate the feasibility of the telescope and make reasonable cost estimates.

Radio astronomy at millimeter wavelengths has developed very rapidly during the last ten years. The spectral range down to $\lambda = 2.6$ mm has been opened, and some work has been done at 1.2 mm. Continuum observations of various galactic and extragalactic objects have yielded much new information and promise to be very important to our understanding of some of these objects. Millimeter-wave spectroscopy has shown the existence of a bewildering array of complex molecules in interstellar clouds, and opened up whole new fields of investigation of great importance to molecular chemistry, the physics and chemistry of the interstellar medium, and star formation.

In spite of the exciting developments in millimeter-wave astronomy in the last few years, and the obvious great potential of this area of research, there are still essentially only three telescopes available for this work--the 16-foot reflector of the University of Texas, the Aerospace Corporation 15-foot reflector and the NRAO 36-foot telescope at Kitt Peak. The small size of these telescopes limits the sensitivity and resolution attainable with them and severely restricts their scientific usefulness.

Further, none operate effectively at as short a wavelength as is now desirable from the standpoint of scientific need, and possible from the standpoint of technical capability. The proposed 25-meter telescope provides a major improvement in sensitivity, resolution and operating wavelength range over existing instruments, and represents a most reasonable compromise between scientific need, technical feasibility and cost.

B. THE TELESCOPE

The proposed telescope is based on the concept of homologous deformation developed by von Hoerner (1967). The general design is derived from that of the 65-meter telescope design (Findlay and von Hoerner, 1972). It consists of a parabolic reflector, 25 meters in diameter, on an altitude-azimuth mount. The reflector surface will be made up of 528 solid surface panels. The reflector support structure is designed to be homologous; the reflector remains parabolic in shape (but may change its focal length) as its aspect with respect to gravity changes. The normal mode of operation will be as a Cassegrain system, with a subreflector 1.4 meters in diameter. Prime focus operation will be possible.

The structural and mechanical designs of the telescope are now well-advanced, and present no particular difficulties. The design specifications for surface accuracy and pointing are somewhat better than the performance of existing instruments but are reasonable expectations in terms of present technology. Several methods for manufacturing surface plates to the required tolerance have been investigated and appear feasible. There is still a large uncertainty in the cost estimate for the plates, which should be reduced through further development work. Another major source of error is in measuring and setting the surface plates in position on the backup structure. A promising new measuring technique has been developed at NRAO by Payne, Hollis and Findlay (1975). It is presently being further refined, and it should provide a sufficiently accurate means of measuring and setting the surface.

All other elements of the telescope structure, drive and pointing system are based on proven designs and components.

To meet the specified surface and pointing accuracies in other than the most benign weather conditions, it will be necessary to house the structure in some form of an enclosure. This is required in order to minimize surface and pointing errors due to wind deformations or thermal gradients in the structure. Two alternatives are being considered; a spaceframe (radome) structure through which all observations would be made, or an enclosure with an aperture that can be closed for protection or opened for observing. The spaceframe alternative has been the most thoroughly investigated of the two, and present cost and performance estimates are based on it.

The second alternative, of an enclosure giving the options of observing through a clear aperture or closed door depending on weather conditions, is attractive in that it would eliminate the non-negligible radome losses for at least some observations. It is probably more expensive than a radome. Further studies of these two approaches must be made.

Telescope specifications and performance are summarized in Table I.1. The telescope and radome designs are discussed in detail in Chapters III and IV.

C. THE SITE

The absorption and emission of radiation by atmospheric water vapor is a major problem for observations at millimeter wavelengths. At wavelengths shorter than 1 mm the effects of water vapor may provide the fundamental limit to the sensitivity attainable with ground-based observations. Therefore, the first criterion for a site is that it should have an atmosphere above it which has a low and stable water vapor content. It should also be reasonably free from clouds. These two requirements suggest sites at a high altitude in the dry southwestern United States, or in Hawaii. A latitude as far south as possible is preferred to allow

Table I.1

Telescope Specifications and Performance

Reflector diameter	25 meters		
Mounting	Altitude-azimuth		
Elevation range	From horizon to 35° beyond zenith		
Sky coverage	Complete, but tracking is not possible within about 1° of zenith		
RMS surface accuracy	$\leq$ 0.075 mm		
Tracking and pointing accuracy	1.2 arc seconds rms		
Slew rates	40° per minute about azimuth axis 20° per minute about elevation axis		
Optics	Cassegrain: magnification = 15.8, subreflector diameter 1.40 meters Primary reflector: f/D = 0.42		
	λ = 2 mm	1.2 mm	0.8 mm
Half-power beamwidth	21"	12"	8"
Aperture efficiency	0.49	0.32	0.15
Radome transmission	0.80	0.75	0.70

better conditions for observing the southern part of the Galaxy, including the region of the galactic center. The meteorological environment should not be so severe as to impair the performance of the telescope, and the site should be in a region where man-made radio noise is (and is likely to remain) low.

Adequate technical support for the telescope and its associated electronic equipment is also very important. The instrument must be maintained, serviced and scheduled to meet the needs of a large number of visiting scientists, and it must be kept at the forefront as a research tool. This requires a skilled technical and operating staff. In order to attract and retain such a staff there should be adequate living conditions near the site and reasonably rapid access to it. Unfortunately the requirement of a high, dry site is generally incompatible with the requirements of good living conditions and easy accessibility, and some compromise may have to be made.

Eight mountain-top sites have been considered for the 25-meter telescope, seven in the continental United States and one in Hawaii. The nature and extent of water vapor data available varies considerably from one site to another. It is not possible, on the basis of existing water vapor data, to select a "best" or dryest site.

Four of the eight sites can be eliminated rather easily, on a variety of grounds. All of the remaining four sites have acceptably low water vapor much of the time and they probably all have very low water vapor some of the time. Thus observations at wavelengths as short as 0.8 mm should be feasible some of the time at all of these sites.

When other factors are considered--latitude, accessibility, radio interference, ease of development--the site in Hawaii appears to be the most appropriate choice for the 25-meter telescope. It is the most southerly of the sites, has a quite dry and stable atmosphere, is already well-developed as an astronomical site, and is relatively easy of access.

The site question is discussed more fully in Chapter V.

D. COST ESTIMATES AND TIME SCHEDULE

Details of the cost estimates are given in Chapter VI. The total estimated cost of the project, including telescope, radome, computer, initial electronics, site development and 20% contingency, is $9.2 million. To this should be added a factor for inflation, to the year of funding. Thus, if the telescope is to be funded in 1978 and if inflation is assumed to be 10%/year, the cost in 1978 will be $12.3 million.

The time required to build the instrument, from first funding, is three years. Thus if funding is provided in 1977, the instrument should be completed and in operation in 1980.

The estimated operating cost is $1.45 million per year.

CHAPTER II

THE SCIENTIFIC NEED FOR THE 25 METER TELESCOPE

A. INTRODUCTION

Radio astronomy has achieved a number of impressive successes in the millimeter-wave portion of the spectrum. These have been gained with equipment which is quite modest in sensitivity and resolving power when compared with instruments now in use, or being built, for centimeter wavelengths. Although progress at millimeter wavelengths is still rapid, we will soon reach the point where little further advance can be made without significantly improved sensitivity and angular resolution. The 25-meter telescope has been designed to meet this need. It will make possible the continued exploitation of already established lines of research, and it will open new areas which are inaccessible to present-day instruments.

The best existing large radio telescopes work well down to wavelengths of about 2 cm, while three smaller telescopes have extended exploration to about 2 mm. Little work has been done in the range from 2 mm to 20 μm; continuum observations in the atmospheric windows at 350 μm and 1 mm have been made largely with instruments not designed for these wavelengths, and the telescopes used in the 20-100 μm range have been limited in size because they must operate from balloons or high-flying aircraft. In all these areas, the sensitivity and resolution are far below what is needed. Yet theory strongly suggests that the most important information on a wide range of astrophysical phenomena is to be found in the spectral region from short millimeter wavelengths to the far infrared.

The sensitivity of a radio telescope depends on the properties of the detection devices as well as on the size and accuracy of the reflector. At the present rate of progress, we can expect a 5-fold increase

in receiver sensitivity in the next five to ten years; any still further increase will be limited seriously by atmospheric effects. Because of the larger size of the 25-meter telescope, its beamwidth will be smaller than that of the NRAO 11-meter telescope (the largest now in use at short millimeter wavelengths) by a factor of 2.3, and its beam area will be smaller by a factor of 5. Because of its more accurate reflector surface, it will be usable to much shorter wavelengths (down to 0.8 mm). It will be far more sensitive to small-diameter sources, and will give much better resolution on resolved sources, than the most powerful existing millimeter-wave radio telescope.

B. CONTINUUM OBSERVATIONS

1. Instrumental Parameters

The 25-meter telescope will be more sensitive than existing millimeter-wave telescopes by one or two orders of magnitude. New kinds of thermal and non-thermal sources will become observable, and better data can be obtained for objects already detected. The flux from optically thick thermal sources increases with the square of the frequency, so they are strongest at very short wavelengths. It is at the short wavelengths that non-thermal sources vary most drastically, and depart most severely from theoretical models.

Continuum observations will be concentrated in the atmospheric windows at 9.5, 3.5, 2.1, 1.2 and 0.8 mm. Table II.1 shows the parameters of the 25-meter telescope at these wavelengths. The rms flux densities and minimum detectable signals at the three longer wavelengths are based on dual-channel, cooled mixer receivers, with system temperatures 50 percent lower than for the 3 mm receiver now in use with the NRAO 11-meter telescope. The figures for 1.2 and 0.8 mm assume bolometric detectors about twice as sensitive as those now available. All of the estimates involve only limited extrapolations and should be quite conservative.

Table II.1

Continuum Parameters for the 25-meter Telescope

	Wavelength				
	9.55 mm	3.5 mm	2.1 mm	1.2 mm	0.8 mm
Half-power beamwidth	96"	35"	21"	12"	8"
Aperture efficiency[1]	0.60	0.56	0.49	0.32	0.15
Radome transmissivity	0.80	0.80	0.80	0.75	0.70
Net aperture efficiency	0.48	0.45	0.39	0.24	0.11
Receiver type	mixer	mixer	mixer	bolometer	bolometer
System temperature[2]	300K	300K	300K	8000K	10000K
Bandwidth	0.5 GHz	0.5 GHz	0.5 GHz	70 GHz	70 GHz
RMS flux density[3]	0.2 Jy	0.2 Jy	0.3 Jy	1.0 Jy	3.0 Jy
Minimum detectable signal:[4]					
(1) 10^m integration	0.05 Jy	0.05 Jy	0.06 Jy	0.2 Jy	0.6 Jy
(2) 3^h integration	0.01 Jy	0.01 Jy	0.01 Jy	0.05 Jy	0.1 Jy

Notes: 1. Aperture efficiency for a perfect reflector is assumed to be 0.60.

2. Double sideband.

3. For 1^s integration.

4. For SNR = 5.

2. Solar System

The sun itself will be an important object for the 25-meter telescope. The beamwidth corresponds to 7×10^4 km at 9.5 mm and 6×10^3 km at 0.8 mm, while the solar diameter is 1.4×10^6 km. Thus photospheric phenomena can be studied in great detail. These include center-limb gradients, the structure and evolution of sunspot and flare regions, vertical structure at the limb, etc. Measurements of circular polarization will give magnetic field strengths, and should show the theoretically predicted spatial displacement between the emission in the two senses of polarization.

The linear equivalent of the telescope beamwidth at the distance of the moon will range from 180 km at 9.5 mm down to 15 km at 0.8 mm.

Measurements of thermal emission through a lunation will place constraints on models of the lunar soil and will show what differences, if any, exist between highlands, maria, and craters. The thermal properties of the larger craters can be mapped in some detail, and the results can be used with infrared and radar data to refine surface models.

It is probable that many comet nuclei can be observed over a considerable range of heliocentric distances, with results which will place strong constraints on models of their structure. In particular, continuum radiation should be observable from the cometary core which contains a high density of electrons, and from at least the inner parts of the dust clouds now known to surround comets. Physical differences between "dusty" and "icy" comets may be elucidated.

Many valuable investigations of the planets and their satellites can be undertaken. Most of these objects will not be resolvable with the 25-meter telescope, but the signal-to-noise ratio will be greatly improved over existing instruments. All of the major planets will be observable (including Pluto at the shorter wavelengths), as will the Galilean satellites of Jupiter, four of Saturn's satellites, and the two dozen largest asteroids. Observations of Mercury, Venus, and Mars over a wide range of phase angles will be important for atmospheric and surface models. Data on the variations of disk temperatures with phase are at present sparse for Mercury, unreliable for Venus, and non-existent for Mars at useful sensitivity. At the shorter wavelengths, the rings of Saturn can be resolved from the main body of the planet, and they should produce a measurable signal which will help in solving the problem of the size and nature of the particles which compose them. It will be possible to observe the variation of the thermal radiation of the Galilean satellites as they enter and leave eclipse; in fact, it will be possible to follow Ganymede and Callisto from ingress to egress with a good signal-to-noise ratio and without serious contamination by the radiation of Jupiter itself. This will provide an excellent delineation of

the thermal properties of their surface. Some useful data on temperature differences between polar and equatorial regions of Jupiter will be possible, for depths into the atmosphere not achieved by other types of observation. These are, of course, only a few of the planetary problems that can be attacked productively with the 25-meter telescope. It is worth noting that a number of the observations mentioned above will be even more valuable if they are made simultaneously with similar VLA observations at centimeter wavelengths.

3. Galactic Objects

Many types of galactic objects are suitable for observation with the 25-meter telescope. They include compact HII regions, structural details of larger HII regions, late- and early-type stars surrounded by dense dust clouds, the dust emission of infrared sources such as the Kleinmann-Low nebula in Orion A, Bok globules, and radio stars (including novae and X-ray sources).

Observations of several of the objects noted above will bear directly on the properties and nature of the interstellar dust, and hence are of importance in elucidating the problems of star formation and the interstellar medium in general. Current models for ionized hydrogen (HII) regions predict a dependence of flux on as much as the fourth power of the frequency at short millimeter wavelengths. Infrared observations of planetary nebulae and late-type stars imbedded in dust show evidence of excess flux, and sensitive observations at short millimeter wavelengths are needed to separate the parts of the radiation which are due to free-free emission and to thermal re-radiation by dust grains. Studies of dense spots in dark clouds are needed in order to determine whether they contain emerging HII regions; data on continuum emission measure, temperature, and density at various short radio wavelengths will greatly assist the interpretation of recent spectral-line and infrared observations. A comparison of the properties of these small, dense knots with those of rather similar larger regions in black molecular

clouds is needed to establish whether there are differences which might account for apparent dissimilarities in the interstellar molecular chemistry in black and dark clouds.

High-resolution mapping of the larger HII regions will reveal the dense spots where star formation may be imminent or in progress. Examination of the interface between the ionized gas and the dense dust clouds known to exist at the boundaries of many HII regions is likely to be rewarding. This is particularly true for the "elephant trunk" structures, columns of dust which are seen to protrude into a number of HII regions. It is important to learn how continuum intensity correlates with molecular emission in order to see whether, as expected, the continuum arises largely from dust grains. We still do not know why the molecules are not all frozen out on dust grains in the very dense clouds near HII regions; high-resolution observations can help determine whether enhanced temperature or ultraviolet radiation within the clouds might be responsible. Similarly, maps of dense ionized knots will provide a means of testing suggestions that they sometimes tunnel through the surrounding dense neutral medium, a mechanism which has been invoked to explain the puzzling presence of blue-shifted optical spectral lines in the ionized gas.

Radio emission from a number of galactic stars has recently been found at centimeter wavelengths. In most cases, the radio emission is strongly and rapidly variable, and the signal strength is highest at the shortest wavelengths. This behavior has been observed in a number of X-ray sources (e.g., Sco X-1 and Cyg X-3) and seemingly normal binary stars (e.g., Algol). Data at millimeter wavelengths are urgently needed in order to find the frequencies where the radio bursts are strongest, and to follow the spectral and intensity evolution of the bursts in sufficient detail to guide theoretical interpretation. A special case of stellar radio emission is seen in the normal novae, several of which have been observed at centimeter wavelengths. At short millimeter wavelengths,

the thermal radiation of the expanding nova shell should become observable within a few hours of the onset of the optical brightening. Thus we have the opportunity to follow in detail the thermal evolution of the nova shell from its birth until it fades away months or years later.

4. Extragalactic Objects

Galaxies of all types and numerous quasistellar objects have been observed over a wide range of radio wavelengths for many years. Their radio properties at wavelengths of a few centimeters and more are now quite well known, although theoretical understanding remains rudimentary at best. To date, accurate millimeter-wave observations have been obtained only for the strongest sources, owing to the sensitivity limitations of existing instruments. With infrared data now becoming available at wavelengths as long as 350 μm, the filling of the millimeter wave gap by the 25-meter telescope will complete the coverage of the spectrum from X-rays and the far ultraviolet down to meter wavelengths, a range of about nine decades in frequency. The millimeter-wave data will be of particular value in the understanding of the radio emission of galaxies in general, since it is in this wavelength range and the far infrared that accurate data will most severely test the theoretical models.

The radiation at millimeter wavelengths comes mainly from dense, compact (angular diameters $\lesssim$ 1 arc second) regions. They are associated with QSO's and the nuclei of galaxies of various types. They sometimes occur in the outer components of extended double sources. Their radio spectra at centimeter wavelengths are often complex, and they often are dramatically variable on a time scale of months to a few years. The variations are sharpest at the shortest wavelengths. Enhanced infrared radiation from these objects is fairly common. It is clear that processes are acting in which there is a rapid release of very large amounts of energy, although their nature is little understood. The variations frequently do not fit current theoretical models, and the sources which

also vary at optical wavelengths generally show no correlation between the radio and optical fluctuations. Progress in understanding these energetic objects requires the constraints which will be imposed by accurate millimeter wave data for a large number of them.

C. SPECTRAL LINE OBSERVATIONS

For spectral line work, the 25-meter telescope is a balanced compromise between the requirements of high angular resolution on the one hand and the need to work at very short wavelengths on the other. We shall discuss the areas of research which can be undertaken in five categories: kinematics and dynamics, kinematics and chemistry, interstellar chemistry, molecular excitation, and hydrogen recombination lines. Most of the observations will be of objects in our Galaxy, although some can be extended usefully to other galaxies as well.

1. Kinematics and Dynamics

This category includes studies of the collapse and fragmentation of giant molecular clouds and the related problems of star formation, of mass out-flow from evolved stars and of gas motions in our own and other galaxies.

Observations of interstellar molecules have, to the present, served one purpose perhaps better than any other: they have indicated the stages through which large tenuous interstellar clouds pass as they collapse and finally fragment into stars or star clusters. This is because molecules alone provide a tool for the study of dense, cool, opaque interstellar clouds. Yet, because of limited resolution, several tantalizing details of the evolutionary process still elude us. Are interstellar molecular clouds governed in their collapse primarily by rotation, by gravitation, or by turbulence set up by internal energy sources? What is the relationship of the OH and H_2O masers with other non-masering molecules in the cloud? And how do molecules in general, as well as the maser sources, relate to infrared objects and to the very small compact HII regions recently found within some giant molecular

clouds by cm-wavelength interferometry. What is the nature of the Herbig Ae and Be stellar emission-line objects, thought to be pre-main sequence stellar objects still surrounded by the placental molecular clouds, and the object of intense study in the infrared and in molecular lines of CO. Intriguing clues about these relationships seem almost within grasp, with current 1 arcmin resolutions, but only for the nearby Orion region. Here, mm-wavelength observations have revealed a rapidly rotating disk in the center of which is the Kleinmann-Low condensed infrared object; this system has a mass of almost 500 $M_\odot$, very similar to that of the Trapezium stars and their associated HII region. Combined with age estimates of the Orion molecular cloud and star cluster, the picture seems to be a region in which star formation has occurred in bursts every 10^5 years, over a period of 10^7 years; at every burst roughly 500 $M_\odot$ out of a total cloud mass of 10^6 $M_\odot$ forms new stars. But we do not know, because of lack of resolution, whether the Orion picture is typical of other regions of star formation in the galaxy. The 5-fold improvement in resolution of the 25-meter telescope will multiply tremendously the number of regions we can study to answer this question.

High resolution as well as higher frequency should allow detection of any super-dense regions in molecular clouds. Such regions must exist since stars are forming in molecular clouds. Thus the final stages of collapse, just before the protostar becomes self-luminous, may be observable with the 25-meter telescope. One particularly interesting hypothesis might be tested, namely that pre-solar nebulae are a major source of interstellar molecules. Even at the small distance of Orion, such a nebula will not be resolved with the 25-meter telescope, but it should be possible to observe a characteristic distribution of molecular abundances and velocities near these objects if they are actually releasing molecules into the overall molecular cloud.

Higher resolution is needed to solve several interesting problems associated with circumstellar molecular clouds and dust shells that surround many infrared stars such as IRC 10216 and CIT-6. One class of problems involves the apparently large mass contained in these shells and how it is maintained in a stable configuration. Higher resolution observations will establish the density distribution in these objects which are 1 arcmin or less in size, and will bear on the question of whether they are releasing molecules into the interstellar medium at significant rates. It will also be important to determine more accurate isotope ratios in these stars, to get further information about the nuclear processes which are occurring there.

In the case of the widely distributed molecule carbon monoxide, the attainable angular resolution can be doubled by the simple expedient of observing the J = 2-1 transition at 1.3 mm; this higher-lying transition has been found to give brightness temperatures comparable to that of the J = 1-0 transition at 2.6 mm. The 25-meter telescope will have a beamwidth of 13" at 1.3 mm; this will permit study of gas motions within 1 parsec of the dynamical center of the galaxy. The transition region between the hot and cold components of the interstellar medium can be examined through observations of "elephant trunks" and rim structures in HII regions, since they are manifestations of interstellar shock phenomena. Finally the spiral structure of other galaxies can be studied, with a higher resolution than can presently be obtained at 21 cm, by using the 25-meter telescope and the CO transitions.

2. Kinematics and Chemistry

The interrelationship between these subjects is shown by the rich diversity of spectral-line profiles in different molecular species, particularly near the cores of the Orion A and Sagittarius B clouds. So far, we have few clues as to why these seemingly disparate objects should be such copious progenitors of new molecules. Significantly improved

angular resolution will permit study of many regions in much greater detail, and thus perhaps to solve this riddle.

The core of the nearby Orion A molecular cloud coincides with the Kleinmann-Low infrared nebula and Becklin's infrared star, which both appear to be deeply imbedded in a rotating, collapsing ridge of some 500 solar masses. At the position of the infrared nebula, unresolved sources of OH, H_2O and SiO maser radiation have been observed over a wide velocity range; curiously, some of the molecular species which have been observed in non-maser radiation have a broad, weak, and spatially unresolved component which almost coincides in velocity with some of the maser profiles. It is possible that there is a hot, dense circumstellar shell near the core of the cloud, and thus it is a matter of considerable interest to relate the origins of the maser and non-maser radiation at millimeter and infrared wavelengths. The center of the Orion A molecular cloud appears to be fragmenting into a variety of smaller clouds whose nature can readily be studied with the 25-meter telescope.

The improved resolution of the 25-meter telescope will almost certainly lead to the detection of new molecules in small dense regions of interstellar clouds. If these regions are at high temperatures (as in the vicinity of protostellar objects such as the Kleinmann-Low nebula), then we may expect to detect many refractory species as they are volatized from the surface of dust grains. Such species as PN, MgO, FeO, HCP, and SiC all require high temperatures to exist in the gas phase; the laboratory spectra of most heavy metal oxides and carbides are only approximately known, and their detection in interstellar space will provide accurate and useful spectroscopic data. The hot, small core may also be a detectable source of maser emission or emission from excited vibrational states in a variety of molecules, and so clarify the true nature of the maser pumping mechanism. If on the other hand the dense regions are at low temperature, very complex species will appear should catalytic

reactions on grain surfaces be important. Examples of such molecules are propynal (CH_3C_2H), heavy alcohols (propyl and higher), alkanes and aromatic rings.

As a final example of the interplay between chemistry and kinematics, we cite the molecular emission of the extended envelopes of the carbon stars IRC 10216 and CIT-6. Here the millimeter-wave line profiles have provided detailed information on the mechanisms of gas and dust ejection from the stellar surfaces into the surrounding interstellar medium. The molecular observations seem to confirm many ideas of the chemistry in a carbon-rich environment which were first explored nearly forty years ago; the molecules we observe must have survived a journey at supersonic speeds out of the stellar atmospheres. The 25-meter telescope will resolve the extended envelopes, permitting better interpretation of several shells detected at near-infrared wavelengths. Thus, the combination of molecular line observations of older envelopes and continuum observations of the younger (a few hundred years) envelopes will enable us to reconstruct the thermal history of these stars over a span of some tens of thousands of years.

3. Interstellar Chemistry

The high angular resolution of the 25-meter telescope will be important in understanding the chemistry of interstellar clouds. Detailed distributions of such molecules as CN, N_2H^+, HCO^+, and HCN are essential in obtaining better estimates of their relative abundances as a function of depth in the cloud. It is already known, for example, that C^+, which is important in current theories of molecular formation, shows a sharp decrease in abundance with increasing depth in the clouds. High resolution observations are also necessary to find if a correlation exists between molecular abundances and sources of ultraviolet radiation, since such radiation may prevent molecules from freezing out on cold dust grains. A correlation in position should also be sought for molecular abundance and infrared sources. In summary, ion-molecule and grain catalytic

reactions will be much better understood when the distributions of molecules are more clearly delineated.

Other sites where molecule formation might occur include the edges of expanding supernova remnants and the bright rims and "elephant-trunk" structures near ionized hydrogen regions. Here again high angular resolution is required to isolate and identify the shock regions.

The chemical considerations discussed so far depend more on the higher angular resolution of the 25-meter telescope than on its higher limiting frequency. The ability to observe at wavelengths of 1 mm and less will bring a whole new class of molecules into radio astronomy, those with only one heavy atom. It will then be possible to observe many of the less dense components of the interstellar medium. Until now, molecules with only one heavy atom generally have been accessible only to optical and ultraviolet observation. But many of their rotational transitions can be observed through atmospheric windows shortward of 1 mm. Table II-2 lists some of the transitions corresponding to wavelengths where the atmospheric attenuation should be under 6 dB at the zenith of a good 13 000-foot site. Because line strength increases strongly with increasing frequency, the light highly reactive species listed in the table can be detected in clouds of moderate density (100-300 hydrogen atoms per cm^3), provided the column density is at least 10^{12} particles per cm^2. This is comparable with the optically determined abundances of CH and CH^+. The importance of the study of molecules in such rarefied clouds lies in the fact that only a limited number of reactions can occur at low densities. If we can understand this precursor phase of interstellar chemical evolution, we will be better able to follow the more complex reactions that occur as clouds contract and become denser.

Because of the high spectral resolution of radio measurements, observations of light species will provide a reliable standard for comparison with optical data. In particular, accurate radio measurements of doppler

line widths will aid the interpretation of many highly saturated ions (e.g., C^+) observed in the ultraviolet. The strengths of MgH and AℓH relative to those of their ions will be sensitive indicators of the ultraviolet and optical fluxes reaching the interiors of medium or dense clouds.

Table II.2

Molecules with Fundamental Transitions
in the Wavelength Range 0.7 mm to 1.2 mm

Molecule	Ground State	Wave Number (cm^{-1})	Wavelength (mm)
MgH	$^2\Sigma^+$	11.4692	0.872
CaH	$^2\Sigma$	8.4593	1.182
NaH	$^1\Sigma^+$	9.667	1.034
AℓH	$^1\Sigma^+$	12.5956	0.794
NH^+	$^2\pi_r$	13.02	0.768
MgH^+	$^1\Sigma^+$	12.6192	0.792
$AℓH^+$	$^2\Sigma$	13.128	0.762
H_2D^+	?	11.488	0.870
CH_2	$^2\Sigma_g^-$	(7.8)	(1.282)
CH_3	$^2A_2''$	(9.57)	(1.045)
PH_2	$^2B_1$	12.312	0.812
PH_3	$^1A_1$	8.382	1.193

4. Excitation Mechanism

Detailed study of the processes responsible for the formation of a molecular line requires that at least two transitions be observed. Current efforts in this direction are hampered seriously by low angular resolution. To minimize assumptions about the brightness temperature distributions, one must compare all lines of a given species at equal resolution, which necessarily is the resolution at the longest wavelength in the set. For CS, with lines at 50, 100 and 150 GHz, excitation studies are now based on a resolution of about 3 arc minutes, which is about half the total angular extent of the higher-lying transitions. Increased resolving power will give a commensurate gain in the understanding of optical depths and excitation mechanisms in molecular clouds, as well as greatly improved estimates of molecular abundances. In the case of polyatomic species with anomalous pumping, such as formaldehyde, high resolution observations will help us to decide which of several competing explanations is most nearly correct.

Finally, we note that the identification of several important species rests solely upon the observation of a single transition. This includes HNC and HCO^+, for example; their identification will not be certain without confirmation by the observation of other transitions which can be reached with the 25-meter telescope.

5. Hydrogen Recombination Lines

Observations of hydrogen recombination lines at the very short wavelengths accessible to the 25-meter telescope will help the finding of relatively cooler and denser condensations in HII regions. The cooler or denser the ionized gas, the higher the frequency where the recombination line to continuum intensity ratio reaches its maximum. Observations at wavelengths longer than 2 cm are sensitive to temperatures around 10 000 K and densities of the order of 3000 cm^{-3}. Recent observations at 3 mm have detected small knots which are cooler ($\sim$7000 K) and denser

($\sim$30 000 cm^{-3}). At 1 mm, knots as small as 0.001 parsec, with temperatures of 5000 K and densities of 10^6 cm^{-3}, will become observable. These may in fact be stars in the very earliest self-luminous stages, or possibly early-type stars still imbedded in a dense molecular cloud. These observations will test current ideas about pre-stellar nebulae, and they might reveal the effects of still-infalling material on the ionized region around a newly born star.

CHAPTER III

THE TELESCOPE DESIGN

A. INTRODUCTION

In the previous chapter the need for a 25-meter radio telescope that will work satisfactorily at 1.2 mm wavelength, and perhaps as short as 0.8 mm wavelength with reduced performance, has been discussed.

The two main mechanical factors which establish the high-frequency limit of a radio telescope are the surface errors of the reflector(s) and the pointing errors. In order that the 25-meter telescope has an aperture efficiency for observations in the atmospheric window at 1.2 mm of at least one-half that of a perfect reflector, the rms (root mean square) surface errors must be no greater than 75 μm (one-sixteenth of the observing wavelength). To avoid further significant loss in sensitivity, and a loss of resolution due to beam smearing in mapping programs, the pointing error should not exceed one-tenth of the beamwidth at 1.2 mm, which is 1.2 seconds of arc. These telescope specifications will allow operation at 0.8 mm wavelength with an aperture efficiency reduced to about 0.15, which will be acceptable for many applications.

Thus the design goals for the telescope are:

Diameter	25 m
Surface error	75 μm rms
Pointing error	1.2 seconds of arc rms

In the following sections of this chapter such a telescope will be described.

B. GENERAL DESCRIPTION

The design of a 25-meter telescope described here is based on the detailed studies by J. W. Findlay and S. von Hoerner (1972) of a 65-meter telescope. The geometry of the 25-meter structure is a scaled down

version of the 65-meter antenna. However, the scaled structure was separately analyzed both by the homologous method and by structural analysis programs used by the construction industry.

Figures III-1 and III-2 show two views of the telescope. It is an altitude-azimuth, wheel-and-track instrument. The entire instrument rotates in azimuth on two circular rail tracks about a central pintle bearing. The reflector rotates about a horizontal axis between the two bearings carried at the top of the support towers. The telescope is driven in azimuth by electric motors geared to the wheels on the azimuth track and in elevation by motors geared to pinions which drive a bull gear on the elevation wheel. Control by a high-speed computer system allows the telescope to slew, scan and track under servo-control at a wide range of rates.

In the wheel-and-track design, the large distance between the two elevation bearings enables the reflector to be supported at a location close to its center of gravity. Hence large counterweights are not required to balance the structure. Counterweights do not add stiffness to a structure, but they require a stiffer, heavier tower design and more driving torque. A common problem of the yoke-alidade design, not present in the wheel-and-track design, is a very restricted space for the drive system; often the gear-reducer must be specially designed to fit into the available space.

For these reasons, all NRAO homology telescope designs have been wheel-and-track, and this arrangement is fundamental to the basic design of all other components of the telescope.

The basic structure of the reflector is an octahedron, one apex of which acts as the feed support, and the other end as a moment arm for elevation motion. The octahedron is formed of, and supported by, the heaviest structural members of the telescope except those of the tower. The elevation axis forms one minor axis of the octahedron, as shown in Fig. III-3. The reflector superstructure is built up from the octahedral

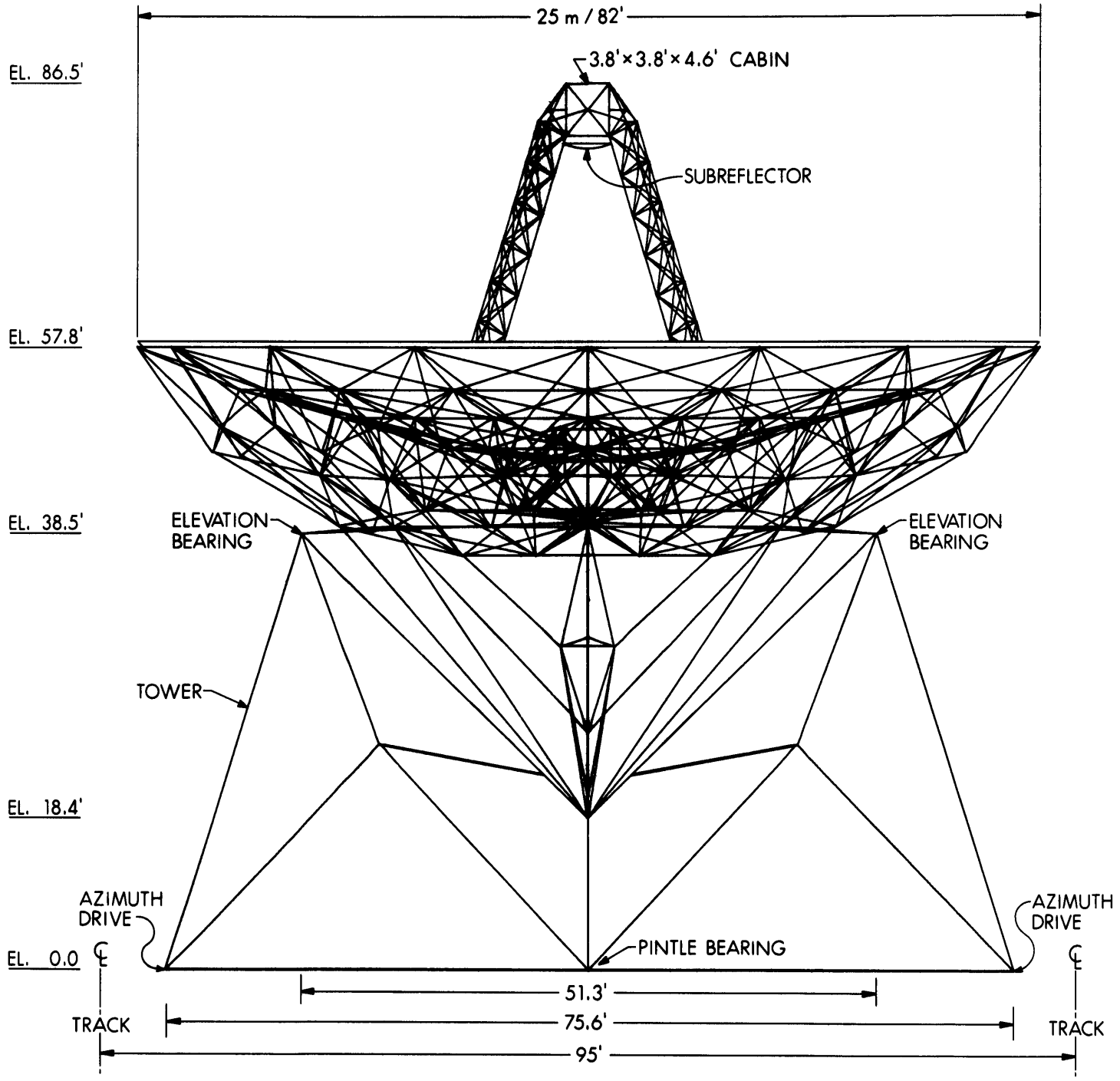

Figure III-1. Front view of the 25-m radio telescope pointing towards zenith.

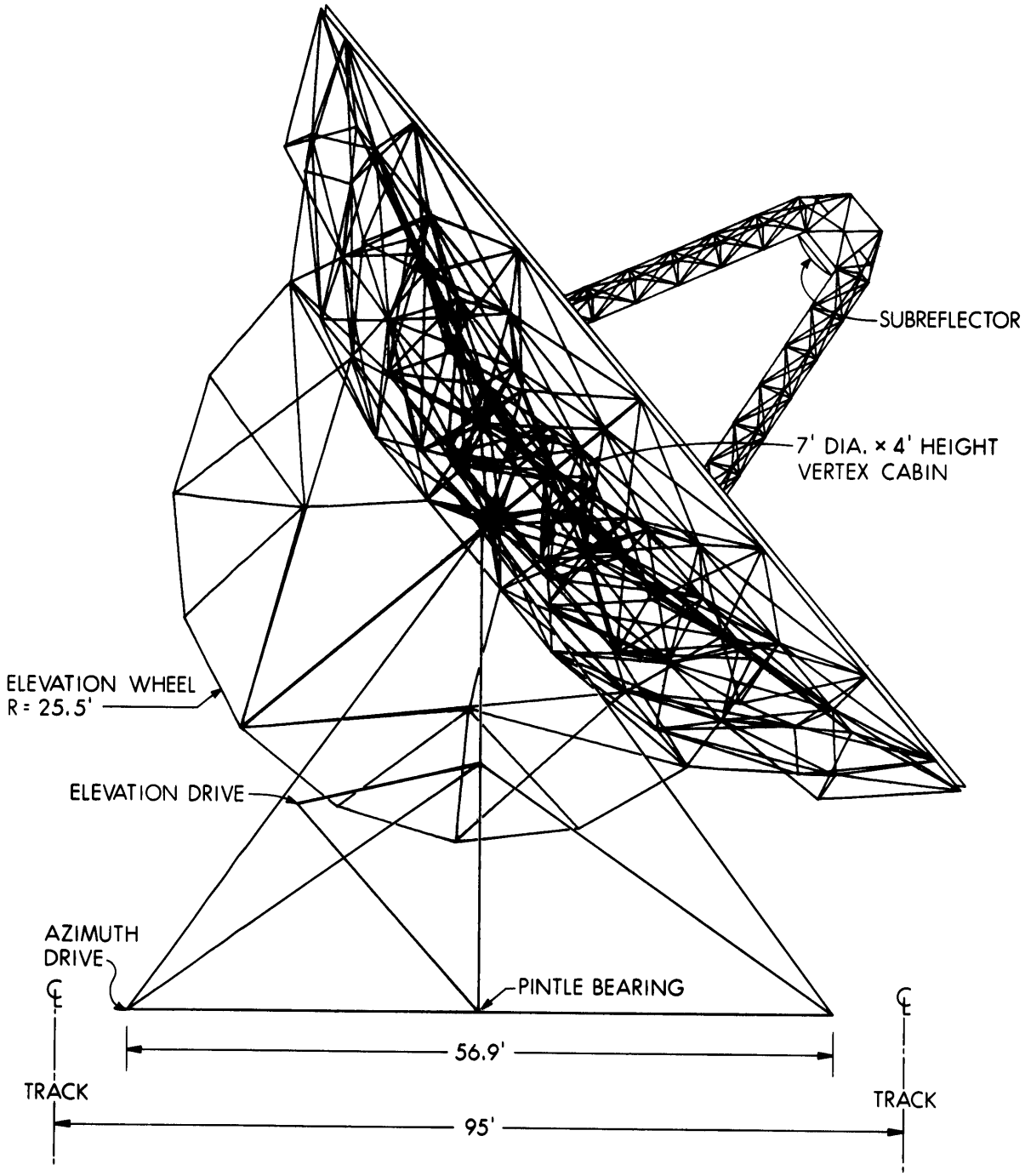

Figure III-2. Side view of the 25-m radio telescope pointing at about 45° elevation angle.

base. A typical arrangement for this superstructure is shown in Fig. III-3(d), using the concept of "equal softness" for all of the surface points of the reflector structure.

The telescope may operate in either prime focus or Cassegrain mode (Fig. III-4). At mm wavelengths, where the size of the Cassegrain subreflector does not have to be large, there are no serious mechanical problems in the use of Cassegrain systems with nutating subreflectors[1]. Cassegrain systems have several advantages over prime focus systems. For continuum work, where variations in the atmospheric radiation and transmission can be a major source of fluctuations, nutating subreflectors provide a very good method of cancelling these fluctuations. The Cassegrain system also reduces the system noise temperature below what is possible at prime focus. It also allows receiving equipment to be placed at the vertex of the dish, where the structural stiffness is much higher than that of the apex of the feed leg structure. This is especially important for the heavy, cryogenically-cooled receivers now in use.

Structural design and analysis have been completed for the tower, reflector backup structure, intermediate (panel) structure, surface plates, and feed support legs. These components have all been completely analyzed with respect to stresses caused by gravitation and wind. The analysis minimizes the deformations caused by these stresses. Three-dimensional frame and truss approaches have both been analyzed using various computer programs. (An IBM 360, Model 65, was used for this analysis.)

C. ANTENNA DESIGN

1. Foundation

The foundation is the part of the structure which distributes the loads at the base of the telescope over a sufficiently large area of the

---

[1] Nutation of the subreflector switches the direction of the beam on the sky. This technique is often used in radio astronomy to cancel noise fluctuations in the atmosphere.

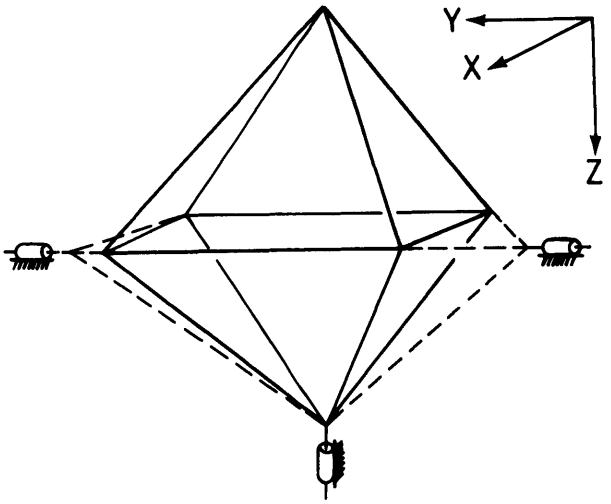

OCTAHEDRON and SUSPENSION

(a)

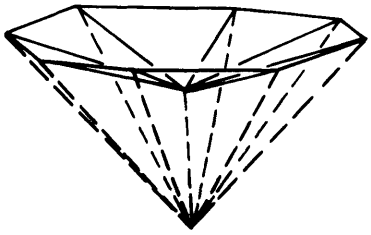

OCTAGON and CONE

(b)

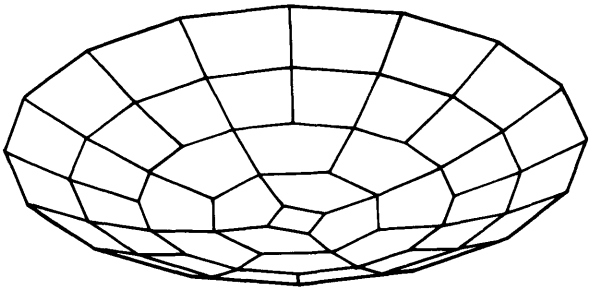

SURFACE PANELS

(c)

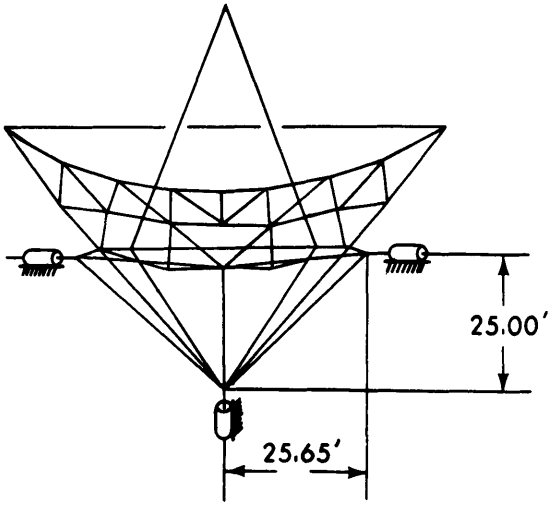

A SIDE VIEW OF THE ANTENNA

(d)

Figure III-3. Three isometric views of components forming the backup structure and one side view of the backup structure.

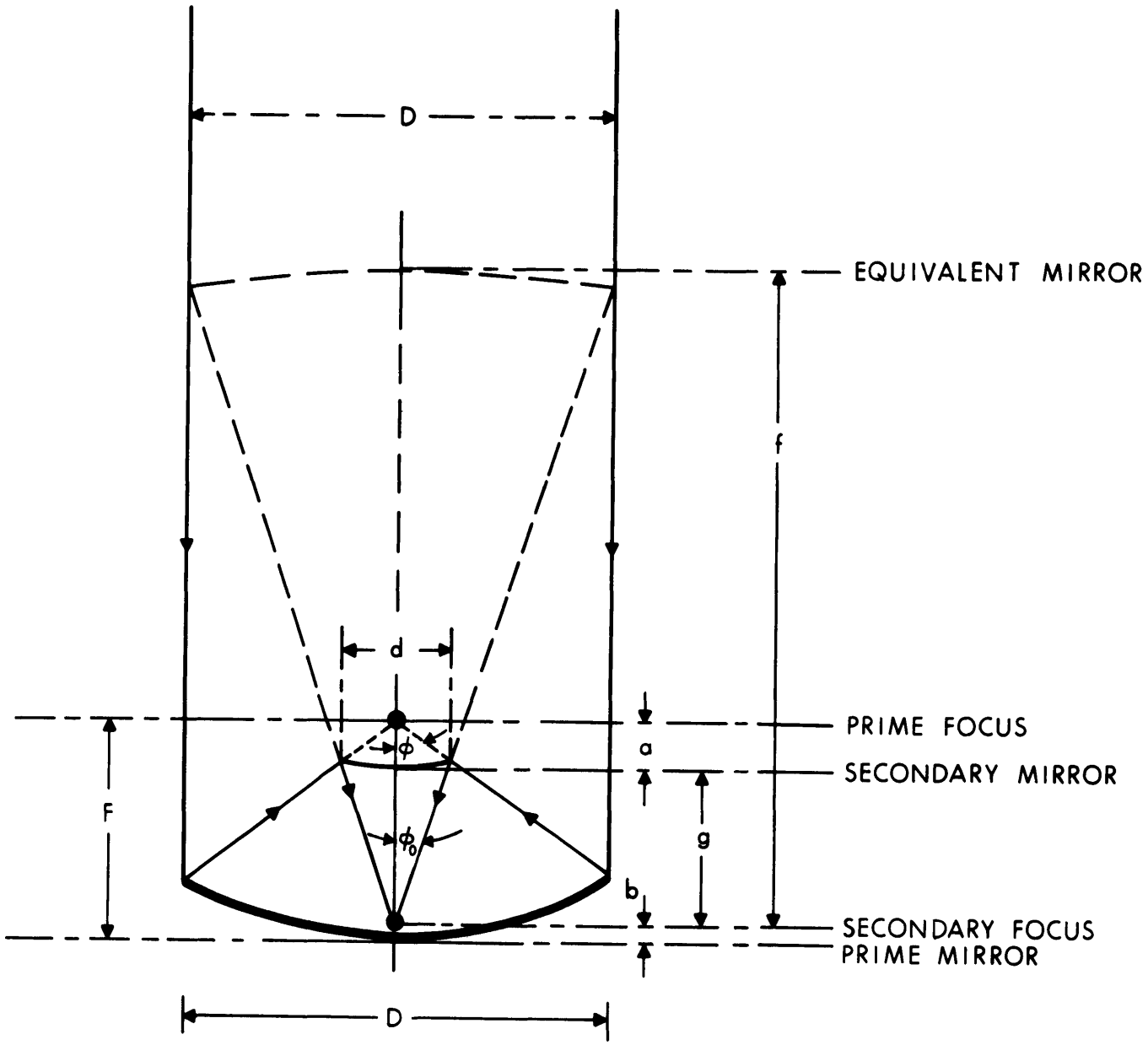

D = 25.0 m
F = 10.5 m
d = 1.4 m
f = 165.9 m
a = 0.6 m
g = 9.5 m
b = 0.6 m

Figure III-4. Optics of the 25-m radio telescope.

soil to reduce the bearing pressure to a safe value. This value varies with the soil conditions and as soon as a site for the 25-meter telescope has been selected, subgrade investigations, including soil type, grain size classifications, dry sample borings and the penetration resistance of the soil, must be made.

The azimuth track will rest on a circular, reinforced-concrete foundation. The concrete will have a minimum ultimate 28-day compressive strength of 3000 psi. The ring-shaped foundation is 8 feet wide and 2 feet deep, with a mean radius of 47.5 feet (Fig. III-5). Two piers one foot in width and 3 feet in depth are built on the concrete base to support two concentric circles of No. 175 crane rail tracks.

In addition to the circular track foundation, there will be a center foundation for the pintle bearing. This foundation supports both vertical and horizontal loads and acts as a reference for the antenna pointing. The vertical loading will be a small fraction of the total load.

The total weight of the telescope is 168 tons. The estimated weight of the foundation is 628 tons. Based on the 95-foot diameter ring-shaped foundation with an 8 foot base width, the estimated static pressure on the soil is less than 0.5 tons/foot^2.

The foundation and rail must not only be strong enough to carry the telescope loads but should also be stable enough to give satisfactory dynamic behavior of the telescope. From both these points of view, the foundation and rail are presently somewhat over-designed, but the design will be reviewed when subsurface conditions at the selected site are known.

2. Azimuth Motion

(i) Azimuth tracks. The cost of the azimuth track will be minimized by using standard, highly hardened crane rail and wheel bases. The two tracks will be welded in circular form and tied to the foundation

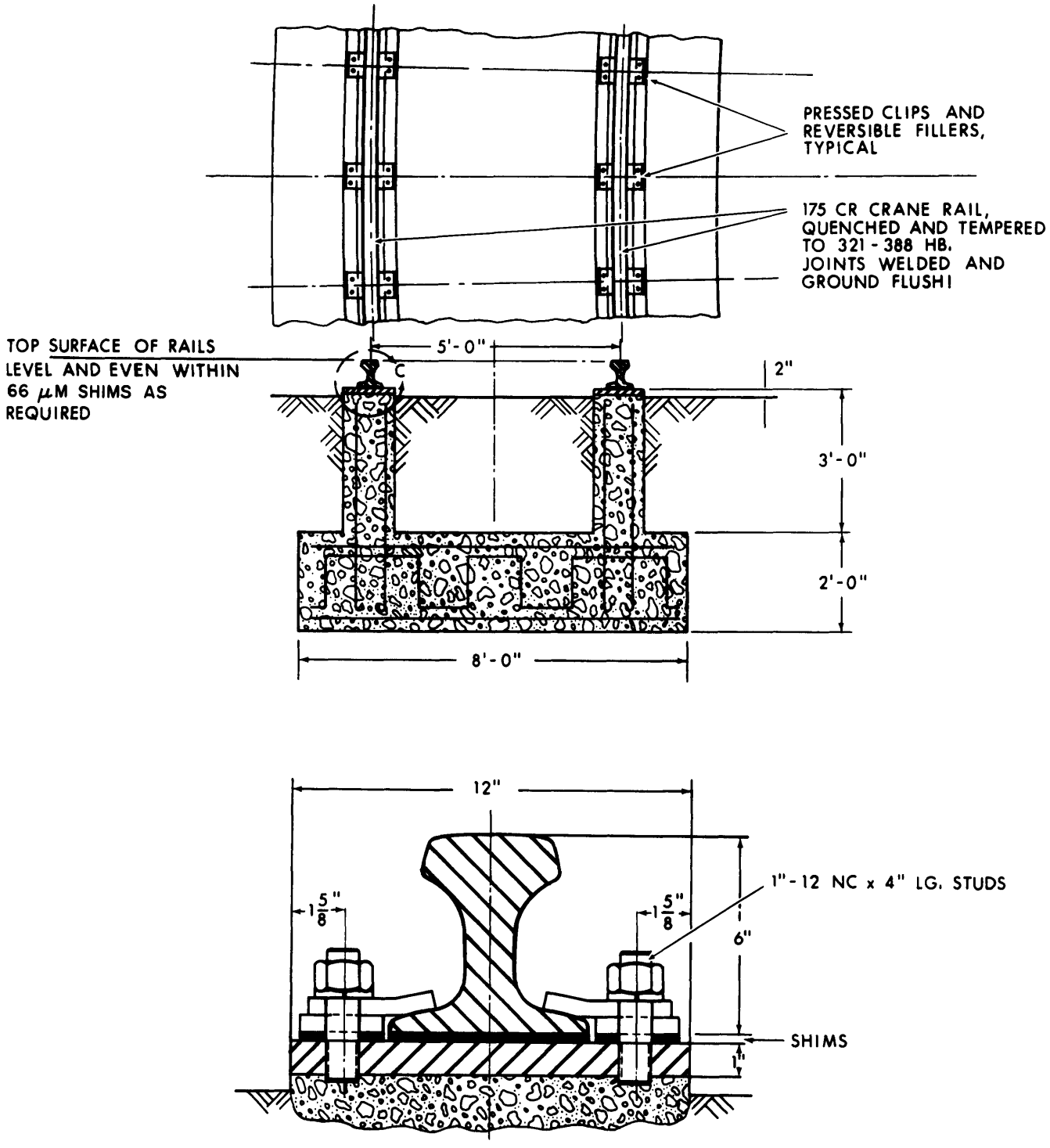

Figure III-5. Cross-section of the foundation and rail for the azimuth track.

by means of pressed clips and reversible fillers. An unevenness of the track, and any difference in level between the two tracks will produce pointing errors of the antenna. The rails will be aligned by the use of shims placed between the rails and the concrete foundation. Experience with a 25-meter communications antenna in Raisting, Germany shows that, with adjustment, an rms deviation of less than 66 μm from the true level is possible, which is acceptable to this proposed 25-meter design. This adjustment was made with the aid of a depth indicator; the reference level for the track was an oil-steadied level of water in a pipe around the track. Pointing errors caused by unevenness in the rail track are repeatable and can therefore be eliminated by calibration.

(ii) Trucks. Figure III-6 shows the truck design. Four trucks, each of which has 4 wheels, share the moving weight and other vertical telescope loads. The trucks will have 7 inch by 12 inch journal axles, 36-inch wheels and 72-inch wheel base. The wheels are driven by gear reducers, powered by D. C. servo motors. Drive motors, gear reducers, brake compressors, etc., are an integral part of the truck assembly. Each truck has a load capacity of 157,000 pounds and thus has a safety factor of 2 if the total telescope weight is carried by the azimuth track. The azimuth locomotion is provided by friction between the driven wheels and the rails. The wheel rims will be hardened according to specifications of the Association of American Railroads (AAR).

(iii) Pintle bearing. The entire telescope structure rotates about the pintle bearing as its center. The bearing is located on the bottom level of the tower. It has to withstand any lateral forces given to the telescope by winds (air circulation) or by inaccuracies in the azimuth track lay-out, which impose small tilts on the telescope structure. It is designed to carry one-third of the total weight. It is a preloaded, self-aligning bearing combination which can take vertical loads and radial loads. The azimuth encoder will rest on an independent foundation,

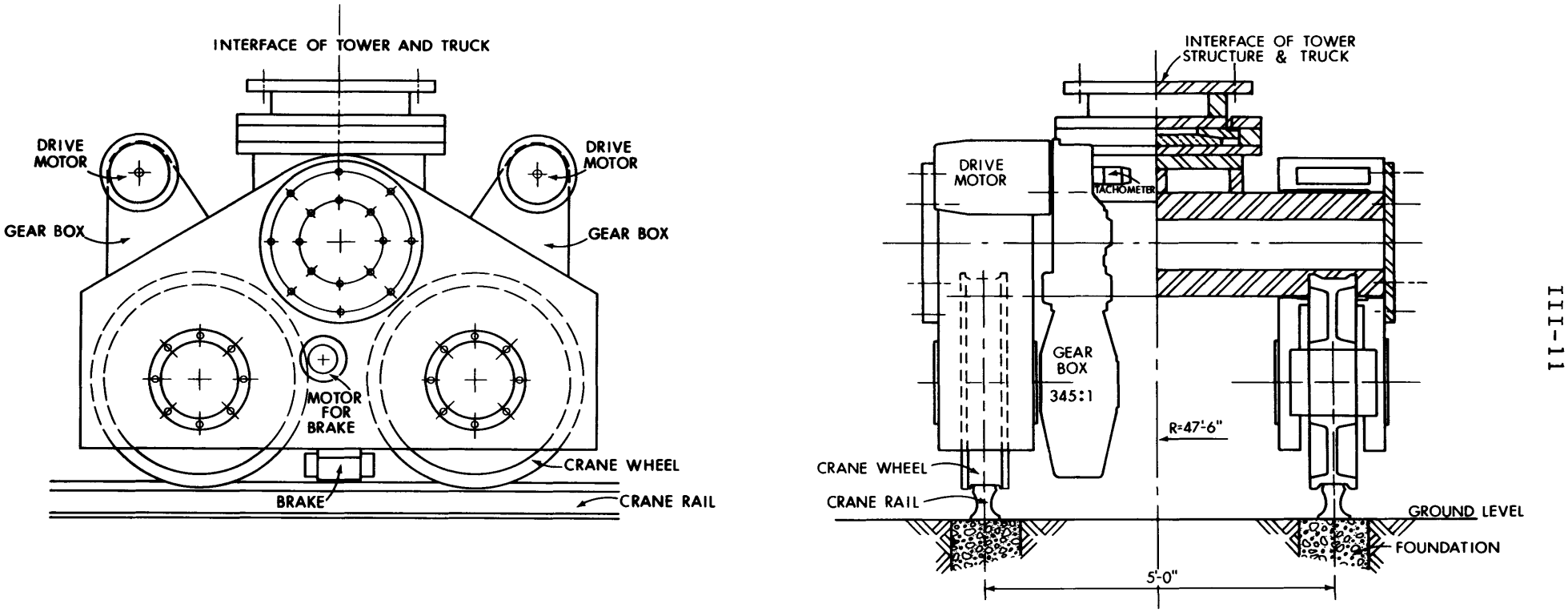

Figure III-6. Proposed azimuth truck design.

within the bearing foundation, and will be coupled via a torque tube to the pintle bearing shaft to obtain the azimuth readings.

3. Tower

The functions of the tower are: (a) to provide supports for the elevation bearings, which carry the reflector structure; (b) to provide support for the elevation drive system, such that a tangential force can be applied to the bull gear of the reflector structure to drive in elevation; (c) to provide connection to the central (pintle) bearing so that the telescope can rotate about a central vertical axis; (d) to provide space for the cable wrap-up, cryogenic equipment, and all necessary electrical cabling; and (e) to provide space for ladders and cat-walks to insure accessibility to areas requiring regular maintenance.

The tower must also (a) have reasonably small deflections due to any external forces; (b) meet the survival loads imposed on it; (c) give a satisfactory dynamic behavior for the telescope structure; and (d) not impose any stresses on the reflector under normal operating conditions which could distort the reflector beyond the limits set by the shortest usable wavelength. Figure III-7 illustrates a tower design satisfying these requirements.

4. Elevation Motion

(i) Elevation drive. The elevation drive carriage and its linkage are shown in Fig. III-8. The carriage is fastened via a pivot to a strut, the other end of which is attached through another pivot to a member of the tower structure. In addition, the gear-drive carriage hangs from two rollers that ride the backface of the elevation bull gear. As the drive turns the bull gear, the carriage can rock on the pivots, thus taking up any irregularities in the curvature of the bull gear. This articulating capability not only absorbs radial variations of the bull gear but also accommodates thermal expansion. Thus highly accurate machining, normally required on elevation bull gears, is not needed. The rocking

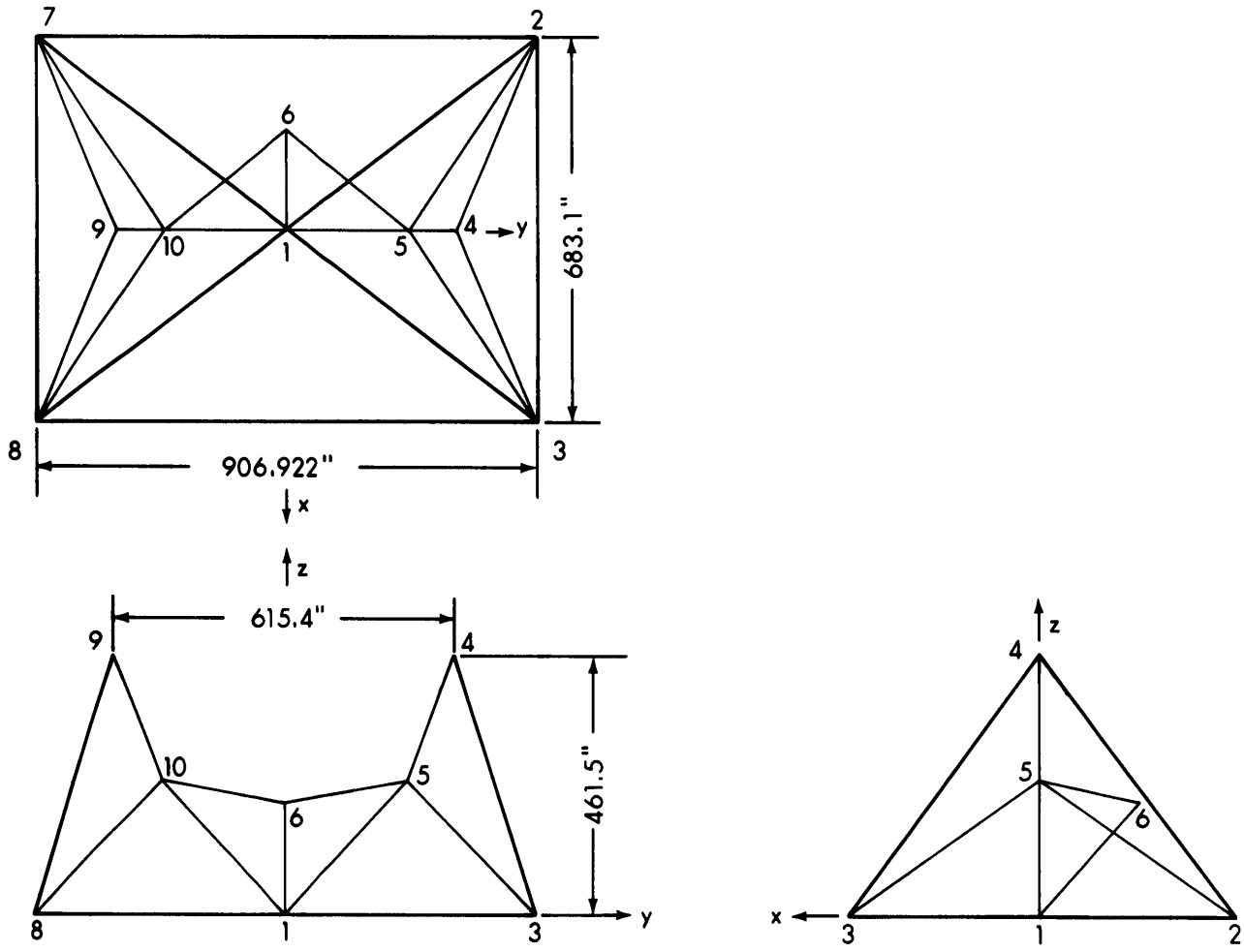

Figure III-7. Three views of the tower design.

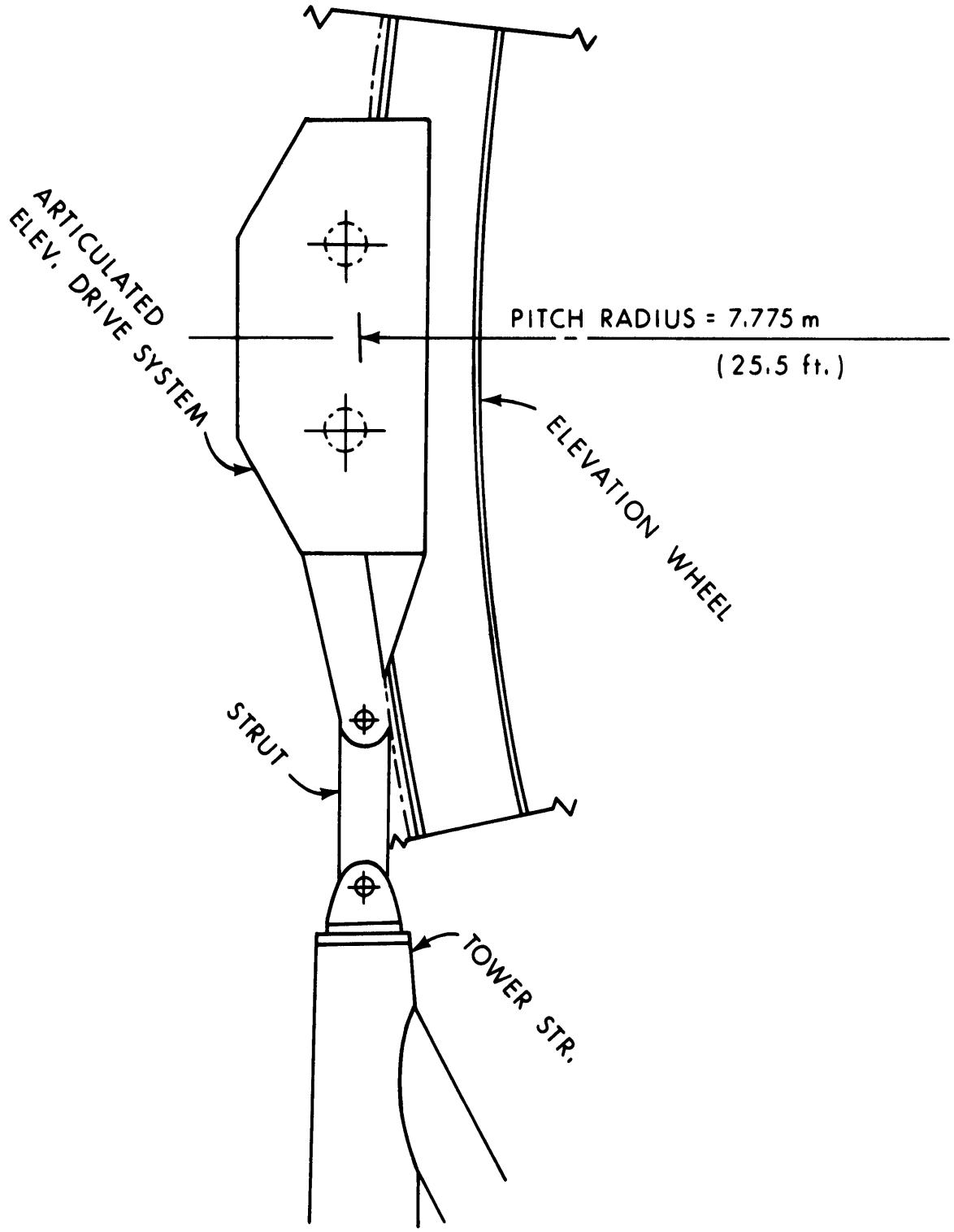

Figure III-8. The elevation drive.

motion of the drive carriage produced by bull gear irregularities will constitute a repeatable pointing error in elevation that may be removed by calibration.

(ii) Elevation bearings. For the optimum performance of the homologous reflector, it is necessary that applied or reactive forces and moments imposed at the elevation bearings be kept at the lowest possible levels in order to minimize secondary, unpredictable surface deformations. In addition, to realize the precise pointing required of this telescope, it is necessary to insure that static friction in the elevation bearings is insignificant.

Preloaded standard self-aligning spherical roller thrust bearings, which primarily act as radial bearings, will be used. The spherical radius is small in order to reduce the frictional torque and a lubricant with a small coefficient of friction will be used.

The total static load in each bearing is 45 tons. The estimated bearing friction moment will be 108 ft-lb. The direction of the bearing friction moment occurs randomly. The position read-out and the distortion of the antenna surface depend on the loading and size of the bearing. Investigation shows, however, these errors are insignificant. With further design and the proper choice of lubricant, this moment might be reduced.

(iii) Elevation shaft encoder couplings. The high angular accuracy of the 25-meter telescope requires a very accurate flexible coupling. It will need to be free of backlash and possess high torsional rigidity, and it must withstand shaft misalignments without introducing large angular errors into the system. Flexible couplings have proven quite successful in many applications. They are not affected by dirt contaminations.

5. The Backup Structure

The backup structure or main reflector structure is supported on the two elevation bearings. The backup structure includes the elevation drive wheel and the feed support legs. It provides 60 homologous points

for the support of the reflector surface. The entire structure is formed by 849 members connected at 174 joints. The 60 homologous points, which are radially symmetrically placed (see Fig. III.10) in turn are bridged by the intermediate (panel) structures which support the surface plates.

The backup structure is homologous. As its elevation angle changes, the 60 homologous points always remain very closely on a parabolic surface. However, the focal length of this surface changes with elevation angle and so does the departure of the direction of its axis of symmetry from the direction defined by the elevation axis position encoder. During observations the gravitational change in focal length is taken into account by a programmed adjustment of the subreflector (or feed in the prime focus mode). The gravitational pointing error is calibrated.

The basic backup structure design is suitable for prime focus or Cassegrain optics. The estimated weight of the stucture is 64,600 pounds.

The structural design of the homology reflector requires an unconventional joint concept. Most structural members connecting at any particular joint are not oriented in common planes, as is the case with most standard space frames, but project from the joints in all directions. In some instances there are as many as 15 members intersecting at one point. Spherical joints are used in this design (Fig. III.9).

The manufacturing tolerance for the location of each joint should not deviate from the design by more than 6 mm (1/4 inch). The structural steel members are designed to withstand the gravitational forces of the structure itself in accordance with the design code of the American Institute of Steel Construction. Thus all members, except for a few of the largest and heaviest, can be obtained directly from commercial steel companies.

The structural members are chosen to meet several additional constraints: (a) the wall thickness of each member should exceed 3 mm (1/8 inch) in order to allow welding; (b) the thermal lag of the entire structure

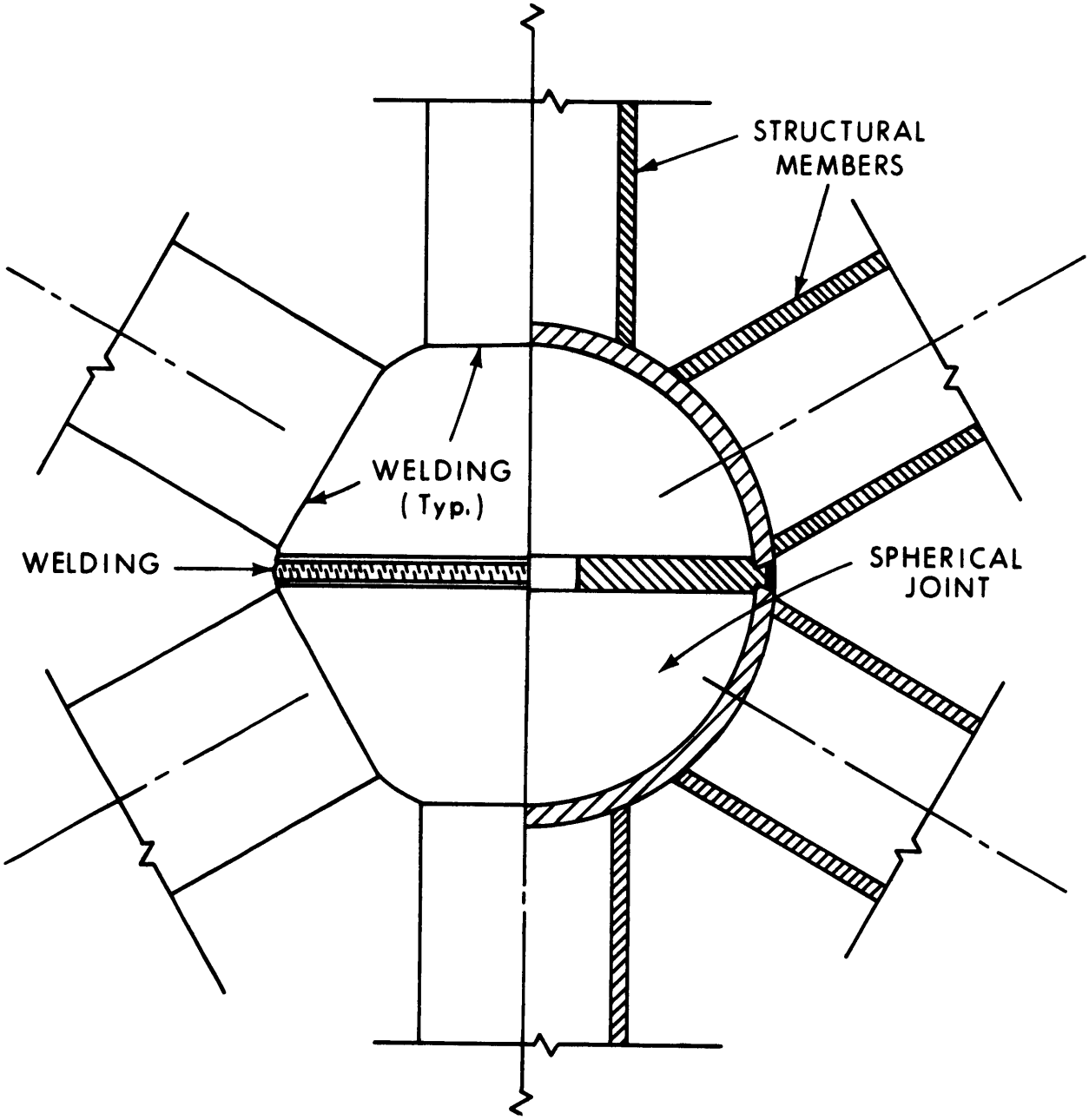

Figure III-9. Spherical joint design.

should be limited to 1/2 hour; (c) local buckling must not occur; (d) no member shall have a resonant frequency which can be excited by expected winds; and (e) under forced oscillation, no member shall suffer overstress at the extreme fiber owing to fatigue.

The designs for both the tower and reflector structure assume the use of a steel of high yield strength. One such type of steel is Cor-Ten, manufactured by U.S. Steel. This type of steel also has good resistance against reduction of cross-sectional area in thin-walled members caused by corrosion of the member interiors. All external surfaces will be protected by paint, which also is used for temperature control.

6. The Intermediate (Panel) Structure

The panels bridge the 60 homologous reflector structure points and carry the surface plates. The panel structures are themselves homologous. The radially symmetric arrangement of the 60 homology points means that four panel designs only are required--an outer ring of 16 (panel A), a ring of 16 (panel B), a ring of 8 (panel C), and an inner ring of 4 (panel D). Figure III-10 shows an isometric view of the geometry for the four panel structures which are arranged radially, forming four concentric rings. Figure III-11 shows the configuration of surface plates upon each panel. There are a total of 44 panel structures.

Structural members of the panels are tubular except for the surface members, which are rectangular. The rectangular bars carry adjustment screws for setting the surface plates. The distance between surface bars in the radial direction, equals the length of the surface plates, each of which therefore rests on four adjustment screws, one at each corner. All structural members are joined together by appropriate angling and welding.

7. Surface Plates

The 25-meter telescope has a surface area of 543 m^2. The parabolic surface is formed by 528 aluminum plates arranged in 8 concentric rings. Each plate has 4 adjustment jack screws, permitting surface alignment.

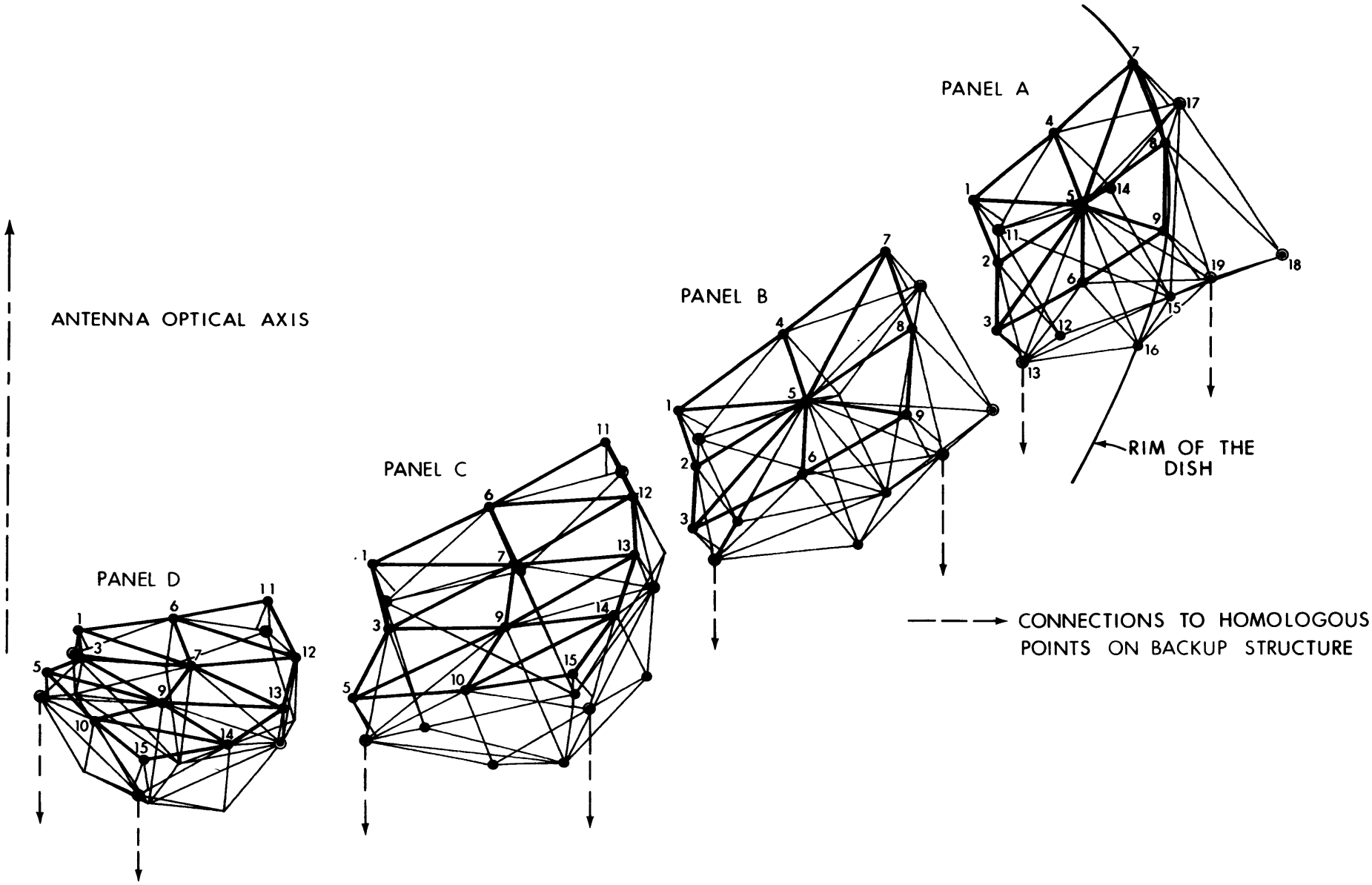

Figure III-10. The intermediate (panel) structures A,B,C,D. The functions of these structures are to bridge across the homologous points and to support the surface panels.

The gap area between the plates is 0.2% of the total surface area. Each of the four panel structures holds two rings of surface plates. Each plate is 1515 mm (59.625 inches) long, measured along the curved plate surface. The geometrical details of the surface plate configuration are given in Figs. III-11 and III-12.

One type of plate, shown schematically in Fig. III-12 was fabricated by Philco-Ford for NRAO. It consists of an aluminum alloy casting surface with a supporting rib structure, the surface of which is machined by a numerically-controlled milling machine. Alternate machining and heat cycling steps were employed to relieve internal stresses produced by the machining.

The second type of plate, designed at NRAO, relies upon surface adjustment by means of screws rather than by machining. A routinely manufactured flat 1/8 inch aluminum skin was fastened to a series of upper ribs which were connected to a stiffer, low-rib structure by 36 adjustment screws. By turning these screws the skin was adjusted to conform to the required shape. Heat cycling to relieve stress was applied between screw adjustments. When the final adjustment was made, the screws were locked by epoxy into final positions. Three of these plates have been built and undergone extensive tests at NRAO. Results are listed in Appendix II.

8. The Feed Support Structure

The function of the feed support is to carry the Cassegrain reflector and all equipment needed for observing with feeds at the prime focus. Both these tasks require that the feed support be stable. Aperture blockage must also be kept to a minimum.

A structure which meets the requirements is shown in Fig. III-13. It will support a payload of 2000 lbs. at the apex. The feed support structure is an integral part of the homology backup design insofar as its weight and stiffness are concerned.

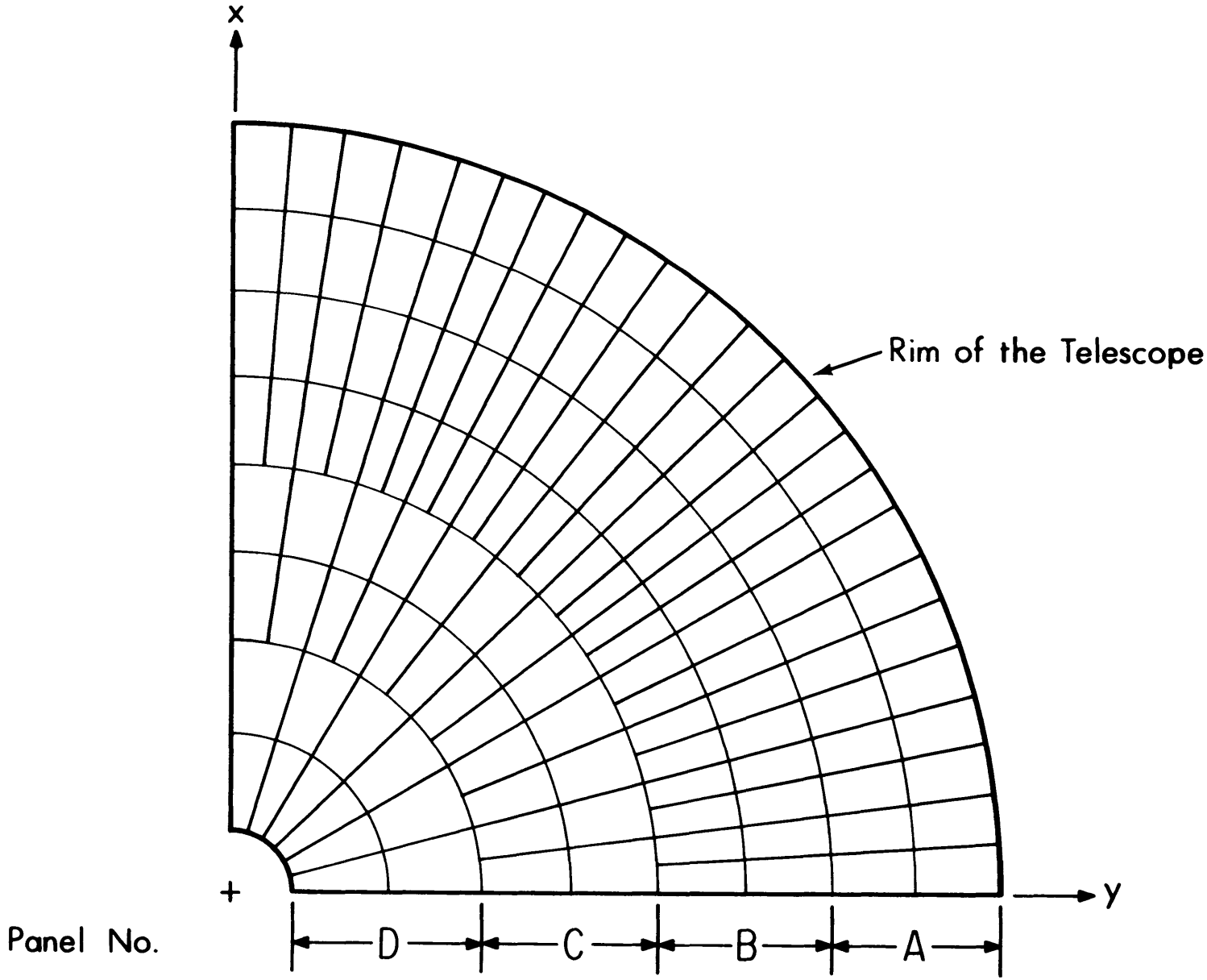

Figure III-11. Surface plate arrangement on one quarter of the aperture.

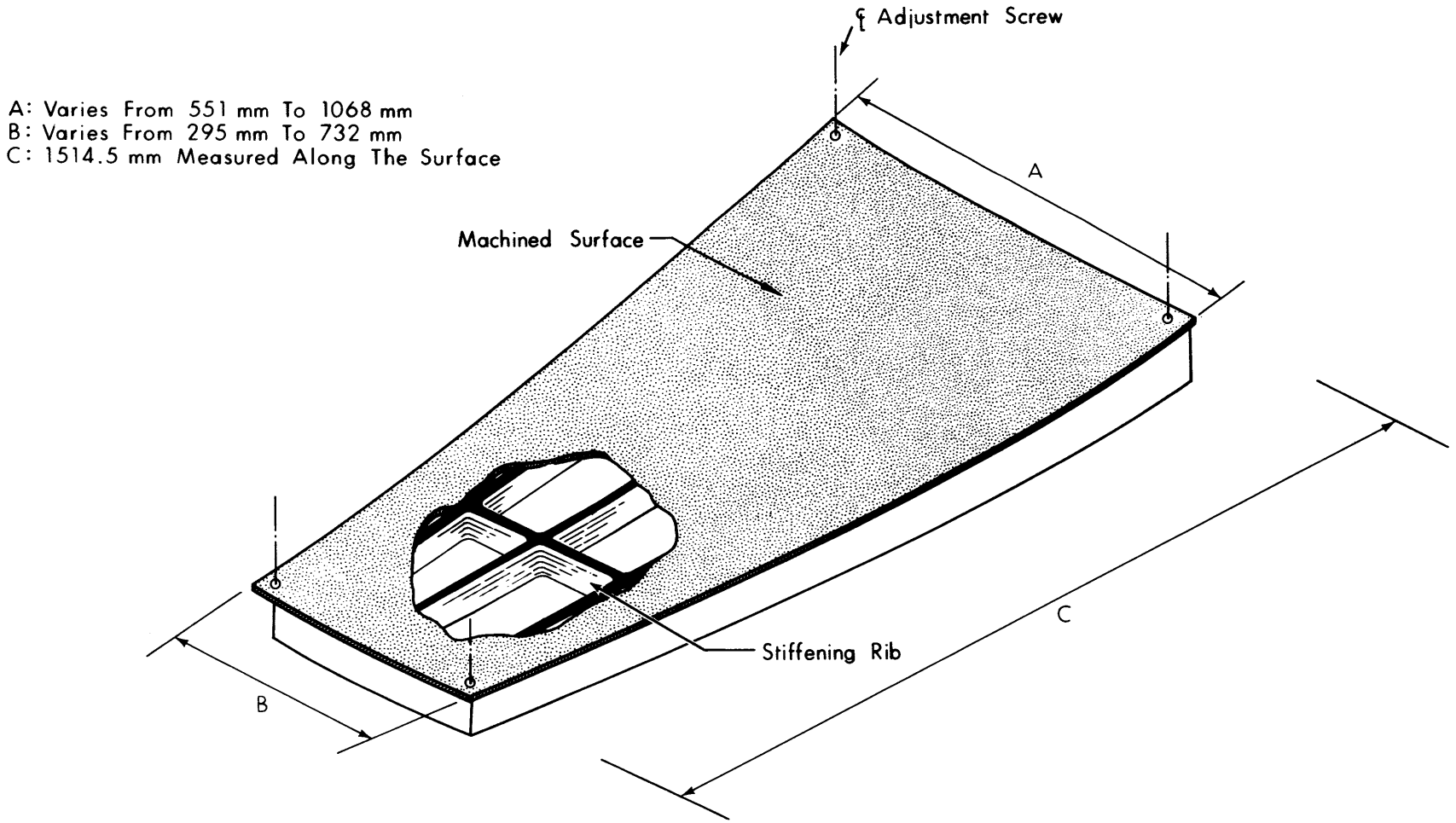

Figure III-12. Dimension and shape of a proposed 25-m telescope plate.

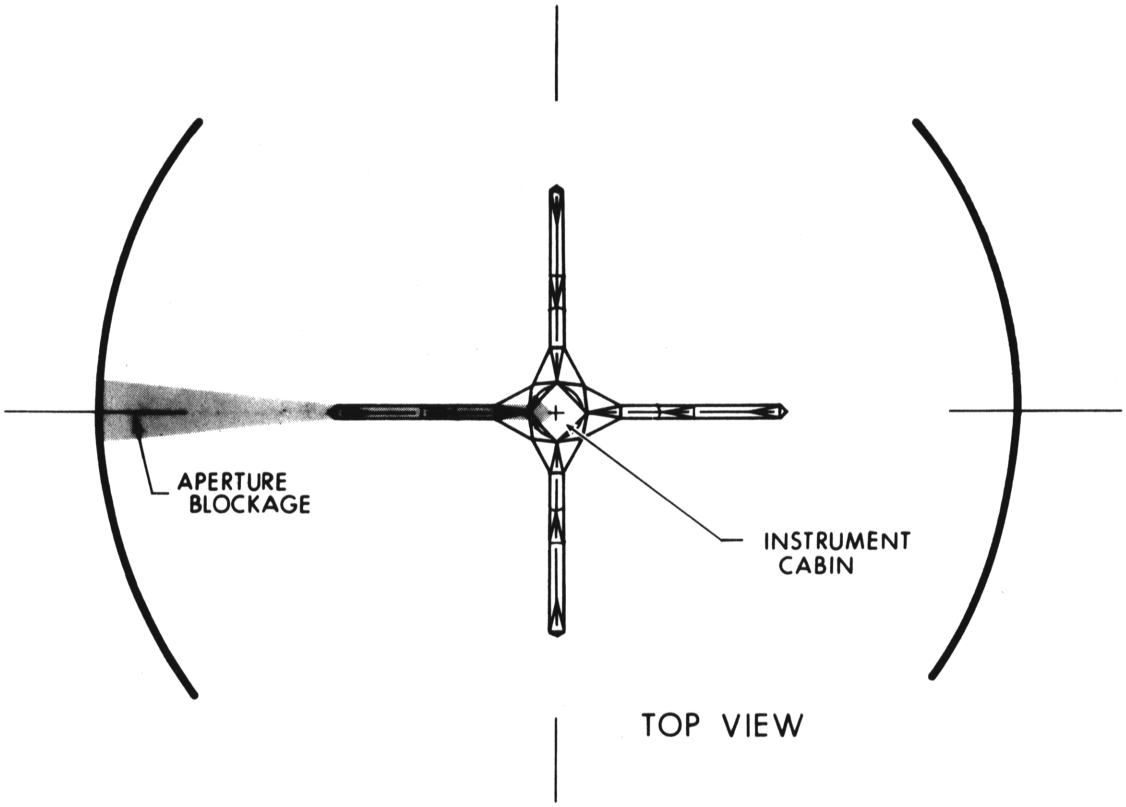

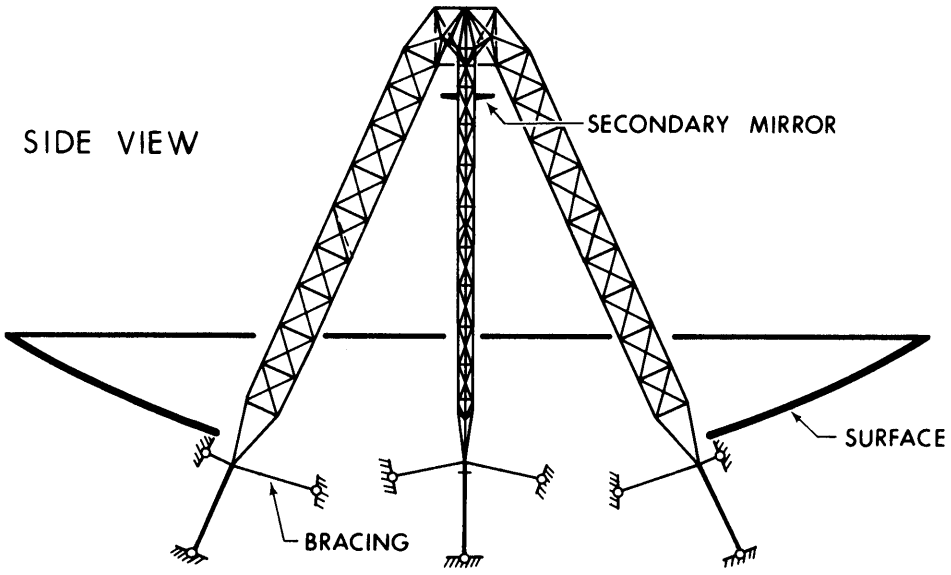

Figure III-13. The feed support structure.

9. The Subreflector

The subreflector will be made of cast aluminum, and the surface milled to the required accuracy by numerically controlled milling machines. The subreflector surface will be attached to an aluminum spaceframe structure to increase its stiffness in order to sustain the high dynamic loading that will occur during nutation, which should be possible at rates up to 5 Hz. Such an aluminum spaceframe support structure would also reduce the surface error of the subreflector under gravity.

The subreflector will be mounted so that it can be removed and replaced readily; this allows a rapid changeover between Cassegrain and prime focus modes. The mounting will allow a range of controlled movements of $\pm$ 15 mm in both axial and lateral directions; it can be rotated and tilted to give a nutating motion. It must be capable of positioning to an accuracy of 250 μm in the axial direction and 130 μm in lateral directions.

10. The Drive and Control System

A block diagram of the drive system for azimuth axis is shown in Fig. III-14.

The telescope rotates on the 29 m (95 foot) diameter azimuth track on four trucks, each truck having four wheels and two motors. This configuration results in an effective gear ratio between truck wheel and telescope axis of 30:1. Each drive motor is geared to an axle by a 345:1 gear box resulting in an overall gear reduction of 10,350:1. To eliminate backlash in the gear trains, the two motors on each truck may oppose each other over a certain torque range. For high accelerations, the motors drive together. In normal tracking operations, however, the motors will be opposing. Directly coupled to each motor is a tachometer that is used to form a velocity servo loop. This velocity servo loop accepts a commanded velocity, in the form of an analog voltage, which is compared with the tachometer voltage, and the difference is used to drive

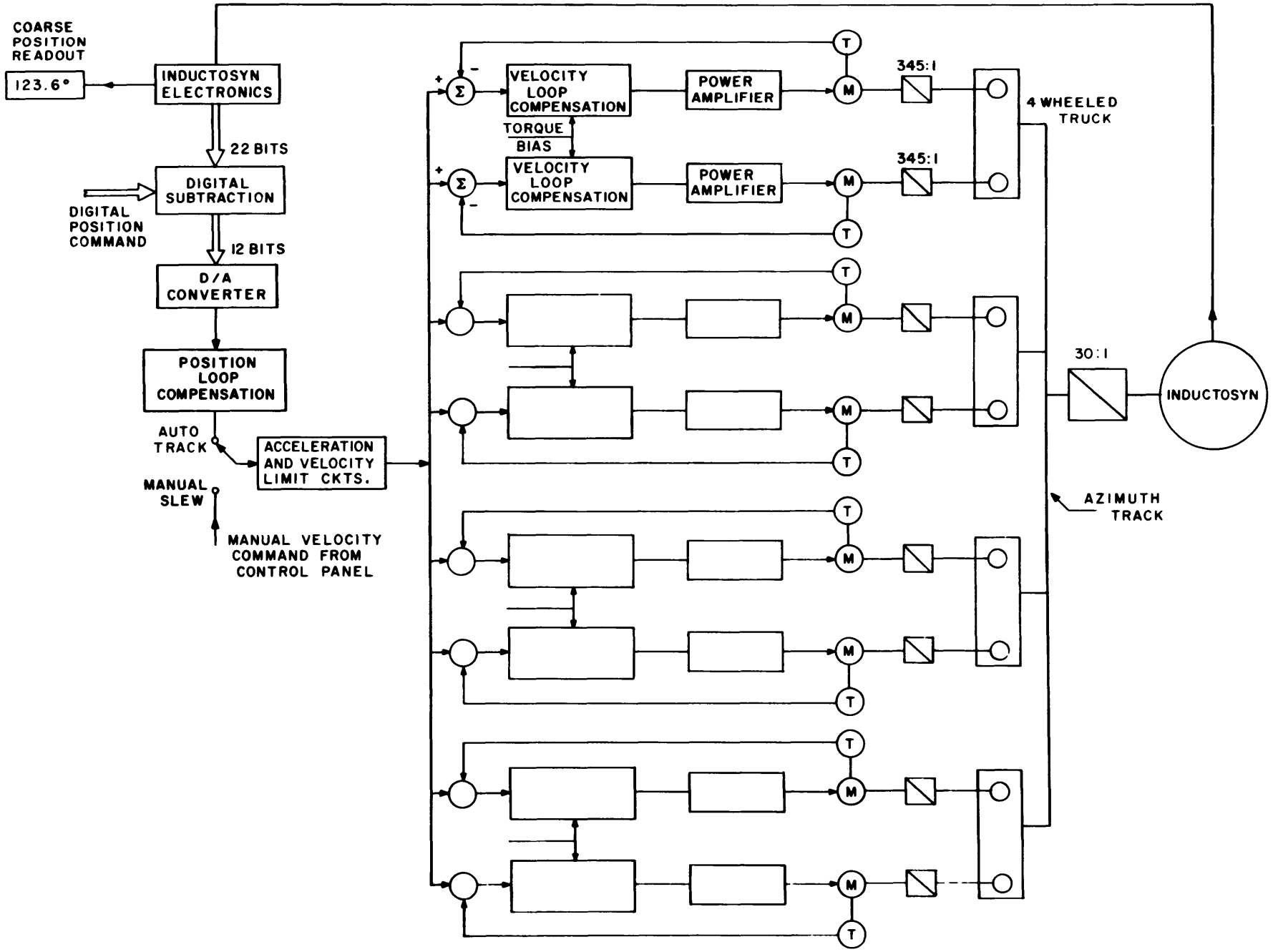

Figure III-14. Block diagram of azimuth drive.

the DC motor through a power amplifier. For the azimuth axis, the speed range will vary from 0 to 40°/min or 0 to 1150 rpm at the motor shafts. The rate in elevation is 0 to 20°/min. To avoid drive-train resonances, the bandwidth of the velocity servo system is restricted to a few hertz.

Permanent-magnet DC servo motors and silicon controlled rectifier amplifiers are chosen for the drive system. It may operate in two modes; auto track and manual slew. In the auto track mode a telescope position is commanded by the computer and is compared with the actual telescope position 20 times per second. The difference between the two positions is represented by a 12-bit number which is converted to an analog voltage and applied to the velocity loop as a velocity command. This forms a closed position servo loop.

In the manual slew mode the telescope operator may generate velocity commands by means of a joystick control on the console to manually drive the telescope to any desired position. A coarse readout on the control console generated from the 12 most significant bits of the position readout permit the position of the telescope to be read to 0.1° for manual drive.

An analysis of the system shown in Fig. III-14 has been carried out, including the effects of inertia and stiffness of the telescope reflector load, stiffness of the gearbox, viscous friction of motors and gearboxes, motor inertia, viscous friction of the load, and inductosyn electronics, in response to given torque requirements (see below). The particular two-integrator (Type II) position loop used in the present design has the advantage of a (theoretical) zero tracking error at constant velocity while generating a constant torque. The bandwidth of the loop is 1.0 Hz. The response of the system to a position step command is satisfactory. For example, 2.0 seconds are required to respond to a 20 mdeg ($\hat{=}$ 1 minute of arc) step command.

An analysis of the errors of this type of system usually concentrates on wind generated torques which will in this case be $\lesssim$ 10 km/h [1)]

---

1) The rate of air movement inside the radome is estimated to be 10 km/h in order to maintain a temperature difference of 0.8° C.

assuming that the telescope operates inside an enclosure. As mentioned previously, a Type II system has theoretically a zero position error under steady tracking conditions and the actual errors will be dominated by breakaway and running friction effects. Position errors during tracking have been analyzed for two NRAO antennas, the 36-foot millimeter-wave antenna and the 45-foot portable antenna. It is found that the tracking errors in both cases are 5-bit peak to peak, giving an rms error of approximately 1.25 bits. We would therefore expect an rms error of approximately 0.1 mdeg (0.4 seconds of arc) with a 22-bit inductosyn, 27 μdeg (0.1 seconds of arc) with a 24-bit inductosyn.

Calculations of the effect of varying drag in the cable wrap and the variation in air circulation around the antenna indicate that errors from both these sources will be negligible.

To achieve the pointing accuracy required, a position encoder with at least 22-bit resolution is needed, corresponding to an angular resolution of 86 μdeg (0.31 seconds of arc).

Optical encoders are available with up to 22 bits of resolution, and inductosyns offer reliable resolution up to 25 bits. An inductosyn utilizes an inductive coupling principle basically more immune to dust and moisture than an optical encoder. The encoder for the elevation axis is directly coupled to the elevation bearing at the end of the elevation axis. The encoder for the azimuth axis is coupled to the tower structure via torque tubes, enclosed by the pintle bearing.

The servo power amplifier uses silicon controlled rectifiers (SCR) which rectify A.C. voltages in such a way that the output is a D.C. voltage related in both polarity and magnitude to the D.C. control-signal input. RF interference caused by the high-speed switching of large currents is a potential problem which can be largely eliminated by switching at the zero current crossing. The non-linear gain characteristic can be minimized by proper design, such as by the use of feedback. SCR amplifiers are reliable and inexpensive.

11. Computer System

The control computer performs the telescope and receiver control functions. It provides telescope tracking and slewing control, and all pointing and other calibration corrections. It must, therefore, respond quickly to telescope and receiver interrupts, and it must have sufficient speed and memory capacity to perform the necessary tracking calculations sufficiently often (every 50 ms). The control computer will also collect the data, perform the necessary translation of the data words and write the data on magnetic tape, and pass the data to the processing computer via a one-way data link. The control computer should have a memory of 128K 8-bit bytes, an effective cycle time of 400 to 600 ns, and it should be 24, 32, 36, or pseudo-32 bit machine, with floating-point hardware. The memory should be expandable to 512K 8-bit bytes.

Figure III-15 describes a possible computer system which would meet the desired specifications.

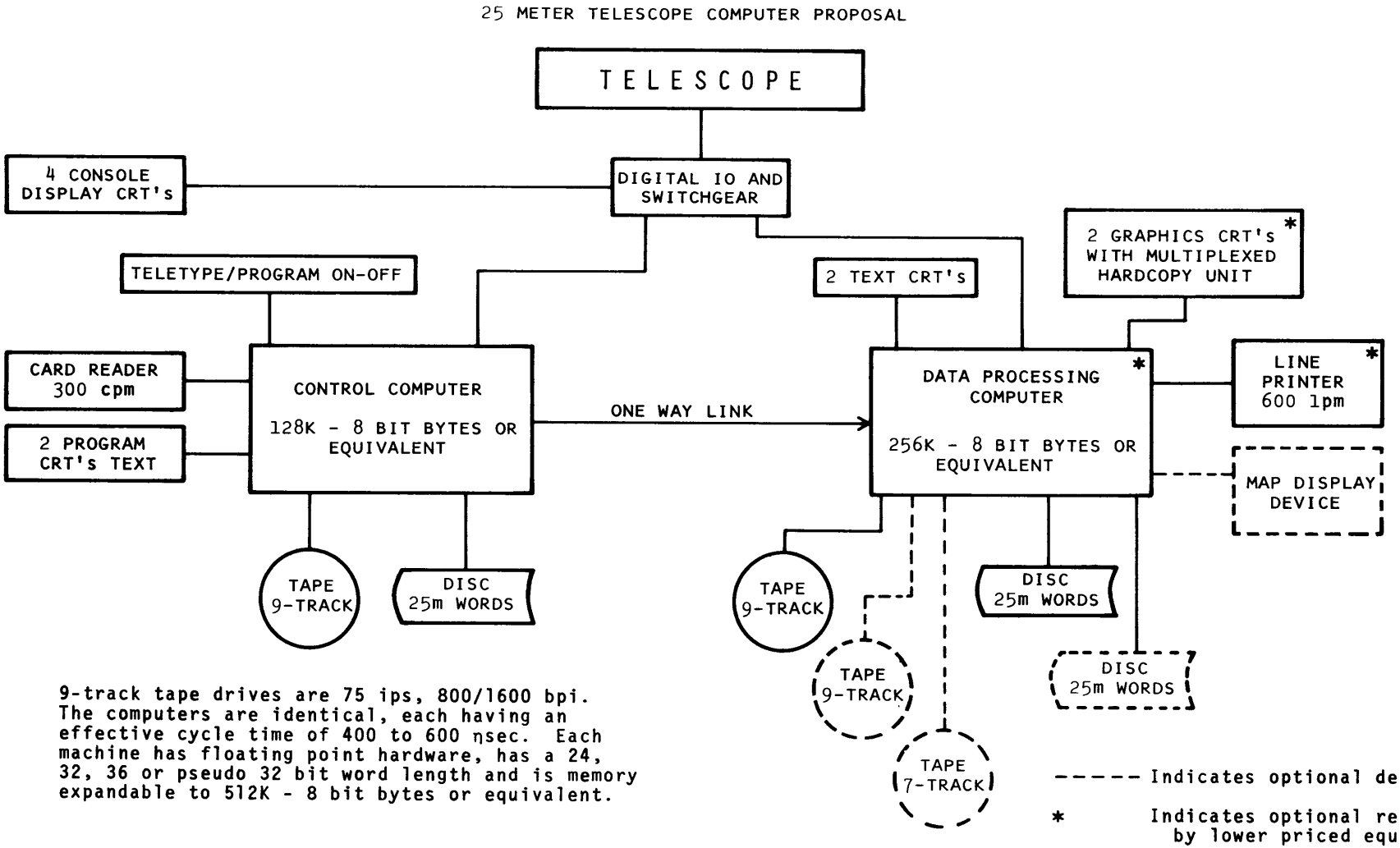

Figure III-15. Block diagram of the 25-m telescope computer.

D. THE MECHANICAL PERFORMANCE OF THE TELESCOPE

1. Introduction

Deformations caused by temperature gradients, changes of gravity, wind, and distortions arising from manufacturing inaccuracies, will all cause deviations from the parabolic surface of a radio telescope. The deformations also cause pointing errors of the antenna RF axis. Various mechanical limitations, such as friction, servo noise, and motor cogging, also contribute to the pointing error. It is necessary not only to predict accurately these limits of performance, but also, through processes of optimization, to minimize the errors.

The static analysis of a structure provides information about deflections, forces and reactions. The dynamic analysis provides information about the dynamic response of the structure under external perturbations. The dynamic properties of the antenna are important not only under wind loading, but also in the design of the servo system. They affect directly the pointing accuracy of the beam while tracking a radio source.

The results of the studies of the 25-meter telescope performance show that it is feasible to build and operate it with a 75 μm rms surface error and 1.2 seconds of arc rms pointing error. Table III.1 shows the expected surface and pointing error budgets under various conditions.

A quick examination of Table III.1 shows that the telescope performance is strongly dependent upon the environmental conditions. The first three columns refer to a telescope operated in the open, fully exposed to sunlight and to wind. During calm, sunny days (column 1) the performance is severely degraded (surface errors around 337 μm and pointing errors of 6.3 seconds of arc). The cause of this degradation is, of course, the thermal distortion of the sunlit telescope.

Even during calm nights thermal effects contribute significantly to the errors, although the telescope then almost reaches the surface error design goals (87 μm vs 75 μm) and actually achieves the pointing

Table III.1

Mechanical Performance of the 25-meter Telescope

	Open			Enclosed
	Noon	Night		
	Calm, Sun	Calm	30 km/h wind	10 km/h wind
Surface Errors	(μm)	(μm)	(μm)	(μm)
Surface Plates	259	73	61	62
Manufacture	40	40	40	40
Gravity	12	12	12	12
Setting	15	15	15	15
Measurements	40	40	40	40
Thermal	252	42	7	16
Wind	-	-	10	1
Panel Structure	29	9	9	7
Manufacture & Gravity	7	7	7	7
Thermal	28	5	1	2
Wind	-	-	5	1
Backup Structure	212	39	20	21
Assembly & Gravity	16	16	16	16
Thermal	211	36	6	13
Wind	-	-	11	1
Subreflector	25	25	25	25
Manufacture & Gravity	25	25	25	25
Total Error [1)]	337	87	70	70
Pointing Errors	(Seconds or arc)	(Seconds of arc)	(Seconds of arc)	(Seconds of arc)
Servo and Drive	0.5	0.5	0.5	0.5
Thermal	6.3	1.1	0.0	0.4
Wind	-	-	3.2	0.3
Total Error [1)]	6.3	1.2	3.2	0.7

1) Total error is the quadratic sum of the individual, uncorrelated, rms errors.

specification (1.2 seconds of arc). A windy (30 km/h in this case) night (column 3) reduces the thermal surface distortions to an insignificant level. However, the pointing error then exceeds the design goal (3.2 seconds of arc vs 1.2 seconds of arc). There is a possibility (not reflected in the table) of stiffening the telescope and tower structure, by adding steel, in order to reduce the pointing errors caused by wind, possibly to 1.2 seconds of arc. The planned telescope is intended to be operated inside an enclosure, and the design of such a strengthened telescope has, therefore, not been made.

The operation of the telescope inside an enclosure (column 4) (radome) permits adequate control of the environment to give the best combined surface and pointing error performance. It will be necessary to create sufficient "wind" inside the enclosure to minimize the thermal distortions. A 10 km/h artificial wind is assumed.

2. Error Contributors

In the following paragraphs the main contributors to the surface and pointing errors given in Table III.1 are discussed in more detail.

(i) Surface errors. The major contributions to the total surface error (which should be less than 75 μm rms) are caused by:

(a) Gravitational deformations. The values given in the table are calculated values using standard structural analysis techniques. The gravitational errors are considered independent of the environmental conditions assumed, and are also not considered to be subject to any significant improvement in future developments of the telescope design.

In a straightforward design the large backup structure would normally contribute a significant amount of gravitational deflection, much larger than the 16 μm given in the table. This is where the homology principle plays its important role in the telescope design. By the correct distribution and dimensioning of the backup structure steel, it is possible to control the deflections caused by gravity. The structure simply deflects into another paraboloid as the gravity vector changes

when the telescope is moved. Theoretically, the gravity deflections may be eliminated, but in practice the necessity of using standard components, the allowance of constructional tolerances, the stability of each structural member, etc., produces a residual deflection, which in the present design is calculated to be 16 μm rms. The panel structure which bridges between the backup and the surface plates are also designed to deform homologously under gravity, reducing the magnitude of the gravitational effect in this part of the structure to 7 μm rms.

(b) Thermal deformations. The thermal deformations are, of course, a direct function of the environmental conditions one assumes. Two thermal situations affect the errors: (1) the temperature difference ΔT across the telescope structure (the thermal gradient) and (2) the thermal time constant of the various parts of the structure dT/dt or $\dot{T}$ (thermal lag). Measurements of these quantities have been made at several observatories for various telescope structures. For outdoor conditions measurements have been collected and analyzed for the 65-meter telescope design (Findlay and von Hoerner 1972). For conditions inside an enclosure measurements have been made at the Brazilian 45-ft telescope, at the NRAO 36-ft telescope, and at the Haystack 120-ft telescope. The results are summarized in Table III.2. The equivalent surface deformations caused by the thermal gradient and thermal lag are given in Table III.3. There is a possibility that the effects of the thermal distortion of the backup structure could be reduced by refocussing the telescope. It is also interesting to note that a moderate wind decreases the surface error by decreasing the thermal gradients across the structure.

(c) Wind deformations. The wind deformations of the telescope surface are relatively small in winds up to about 30 km/h. The wind distortion is dependent on the direction of the wind and the values used are average values. The worst case wind distortion is about three times higher.

Table III.2

Thermal Environment for 25-meter Telescope

	← Open →			← Enclosed →
	Day	Calm Night		
	Calm, Sun	Midnight	After Sunset	10 km/h wind
Thermal Gradient ΔT	(°C)	(°C)	(°C)	(°C)
Backup structure	5.0	0.8		0.8
Panel structure	5.0	0.8		0.8
Surface plates	6.7	1.1		0.8
Thermal Lag $\dot{T}$		(°C/hr)	(°C/hr)	(°C/hr)
Backup structure		0.8	4.8	0.8
Panel structure		0.8	4.8	0.8
Surface plates		0.8	4.8	0.8

Table III.3

Surface Errors Caused by Thermal Effects

	Thermal Gradient	Thermal Lag
	(μm/°C)	(μm h/°C)
Surface plates	37.8	$\approx$ 0
Surface panels	5.4	1.8
Backup structure	37.8	19.8

(d) The surface plate and subreflector manufacturing errors. The potential contribution to the surface error by manufacturing tolerances has not been firmly established. Measurements of the surface errors of two cast aluminum plates made as prototypes for the 65-meter telescope show an average surface error of 59 μm rms. One of the plates measured 41 μm. One potential manufacturer claims that by using a servo-controlled milling machine, 25 μm might be achieved. It therefore seems reasonable to assume that by sufficient care and by employing a servo-controlled milling machine one should be able to consistently produce surface plates with a manufacturing error less than 40 μm rms. This value is, therefore, used in the error budget for the proposed 25-meter telescope.

The Cassegrain subreflector should ideally have a smaller surface error than the main reflector panels. Since only one subreflector is required, one can afford the extra care and effort needed to achieve the best possible surface. It is therefore reasonable to expect 25 μm rms as the manufacturing surface error for the planned telescope. Presently the NRAO 11-meter millimeter wave telescope has a subreflector with 50 μm rms surface errors.

(e) Surface measurement and adjustment errors. The error in the measurements of the telescope surface is, as can be seen in the tables, a significant part of the total error budget. Several methods have been developed and used to measure various telescopes. The method described in detail in Appendix I seems to be the most accurate available today. It has been successfully used on the NRAO 11-meter telescope with an estimated measuring error of 50 μm. Several possible improvements of this technique have been suggested, and it is estimated that 40 μm can be achieved with reasonable care. This is the error assumed for the planned telescope. There is potential for still further improvements, and 25 μm should be possible in the future.

The precision of adjustment of the surface plates also contributes to the total error. The 25-meter telescope will have more than 2000 adjustment points and a semi-automatic adjustment tool has been designed (Appendix V). The adjustment precision of this tool is estimated to be 15 μm.

(ii) Antenna pointing errors. The pointing errors of a radio telescope may be divided into two categories (1) repeatable errors that can be reduced to an insignificant value by proper design and calibration, and (2) random errors that cannot be reduced or eliminated by calibration. At 1.2 mm wavelength, the antenna beamwidth is about 12 seconds of arc. It is desirable that the random pointing errors be less than 1/10 of the beamwidth or 1.2 seconds of arc rms. There are three main contributors to the pointing error budget.

(a) Servo and drive pointing errors. The analysis of the proposed servo and drive system show an error less than 0.5 seconds of arc when 22-bit encoders are used.

(b) Thermal pointing errors. Both the thermal gradient across the telescope structure ΔT and the thermal lag $\dot{T}$ cause random pointing errors. For the environmental conditions that exist inside an enclosure with a 10 km/h air movement, the thermal contribution to the random pointing error is 0.4 seconds of arc. Higher thermally induced errors occur for a telescope which is exposed to the sun on a calm day (6.3 seconds of arc) and is one of the reasons for operating the planned telescope inside an enclosure.

(c) Pointing errors caused by wind. The pointing errors caused by wind are calculated to be 0.3 seconds of arc for the 10 km/h wind inside an enclosure. However, the higher wind of 30 km/h one will often encounter in the open, will increase the wind-induced pointing error to 3.2 seconds of arc. A telescope specifically designed to operate in the open might achieve lower wind-induced errors by adding steel to the structure.

3. Summary

Achievement of the performance goals of the 25-meter telescope requires only a modest improvement over what has already been achieved in the areas of manufacturing tolerance and measurement. Existing, standard techniques can provide a surface with total error of 98 μm (rss). An accuracy of 70 μm appears readily attainable, while with still further improvements, mentioned above, a 55 μm rss surface error can be attained.

APPENDIX I. SURFACE MEASUREMENT TECHNIQUES

This appendix is a condensed version of a report by J. M. Payne, J. M. Hollis and J. W. Findlay (1975). It describes the most accurate method presently available for measurement of antenna surfaces.

A. INTRODUCTION

Over the past few years we have investigated various methods of measuring high-precision antennas. Our previous approach to the problem has been confined to investigating methods of measuring distances as accurately as possible. The antenna surface may then be surveyed by measuring distance between many points on the surface and one or two reference points. For measuring the 25-meter antenna the accuracy required of these range measurements is generally better than 0.05 mm at ranges up to about 20 m.

Two methods have evolved from this work. The first uses a microwave method to measure distances from the focal point of the antenna to transponders on the parabolic surface. This is a useful technique for measuring the deformations of the surface that may result from movement of the antenna or changes in ambient temperature. However, for various reasons this method is not well suited to the measurement of absolute distance so necessary for the initial setting of the antenna.

The second method uses a modulated laser beam to measure distances from both the vertex and the focus of the antenna to optical corner cubes on the surface. The required accuracy of the range measurement is achievable and this method is certainly feasible. Obvious disadvantages are the need for many corner cube reflectors, a system for steering the laser beam to different reflectors and an efficient data collecting system.

The method mow described uses a completely different principle The curvature of the surface is measured with a high accuracy at many points along a radius of the surface. These curvature values are then

integrated twice with respect to the distance along the surface by an on-line computer, the result being the y coordinate of the surface as a function of the distance along the surface. This is repeated for different radii and a contour map of the surface generated.

B. THE PRINCIPLE OF THE METHOD

The theory of the method is simple. In the following Fig. III-16(a), let OS be a line in the surface to be profiled. The curvature, K at any point P

$$K = \frac{d\theta}{dS} \tag{1}$$

where θ is the angle the tangent to S makes with OX. Thus, at point P

$$\theta_P = \int_0^{S_P} K \, dS \ . \tag{2}$$

If K is measured continuously, or nearly continuously at equal small steps of size ΔS in S, from the origin to point (P), then θ_P can be derived from equation (2). The initial conditions at the origin are, for a parabolic surface of revolution, $\theta = 0$ and $S = 0$.

For every point at which (2) is evaluated, we have

$$\sin \theta = \frac{dy}{dS}$$

and hence

$$y = \int \sin \theta \, dS \ . \tag{3}$$

Hence, y may be computed by a second integration as a function of S. Again, the initial conditions at the origin are $y = 0$, $S = 0$ for a near parabolic surface of revolution.

C. THE MEASUREMENTS

The machine which measures K and S is shown in principle in Fig. III-16(b).

It is a three-wheeled truck, with a very precise depth transducer mounted at its center. The front single wheel has attached to its shaft an encoding transducer which gives a TTL pulse 250 times for each wheel rotation. Each pulse represents a change of S of an accurately fixed amount (in the device tested S was 0.6384 mm). The computer measures S by counting pulses from this wheel transducer. Each wheel pulse also interrogates the depth transducer and reads the depth transducer reading into the computer. If the distance between the front and back wheels equals L cm and the transducer reading is d cm (read as the depth below the plane on which the three wheels rest) then the curvature K is given by

$$K = \frac{8d}{L^2 + 4d^2} \quad . \tag{4}$$

A computer was used to derive K values for each S value from 0 to the end of the track. It performed the integrals (2) and (3) in real time and stored the data. When all tracks had been profiled the computer assembled all the results and performed the necessary data reduction to draw a contour map of the reflector surface.

The machine was built and tested by making profiles at 23 radii of the 36-foot radio telescope operated by NRAO on Kitt Peak, Tucson. The computations were performed by the telescope computer.

D. THE ACCURACY ACHIEVED

Two sets of measures of the 36 foot surface were made--these were independent and taken radius by radius with a time interval of about 10 minutes between the runs. They were integrated separately to give two sets of values for the coordinates of 483 surface points. To estimate the measurement accuracy (which we call M), we calculated

$$M^2 = \frac{1}{N} \sum_N \left\{ (Z_1)_i - (Z_2)_i \right\}^2 \tag{5}$$

where $(Z_1)_i$ $(Z_2)_i$ are the measured Z coordinates for the ith point as derived from runs Nos. 1 and 2, respectively. (Z is measured parallel to the reflector axis.)

We find M = 0.05 $\pm$ 0.01 mm for our results, which suggests that the random measurement error for an 11-meter dish is about $\pm$ 0.050 mm.

E. DISCUSSION

The 25-meter telescope requires a measurement error of about 0.040 mm. We do not at present claim that the above system would achieve this result at the 25-meter diameter, but we note the following:

(a) Our measurements were made with the first model of the trolley ever to be built. It may be possible to improve the trolley.

(b) Our tracking on the reflector was not perfect; thus the x,y coordinates of our ith point on the 2 runs may have been different. This can be improved.

(c) Even in the short time between runs the dish temperature (and shape) changed. We have evidence of a 0.10 mm change of Z at the dish edge on one pair of runs taken 10 minutes apart. Some part of our measure of M will have been due to temperature changes.

(d) In a later repeat of the measurements, made in October 1974, 48 radii were measured in less than 4 hours work. Since this work was designed to measure the telescope and not to determine measurement accuracy, we cannot easily state that accuracy. However, the speed at which more than 3×10^5 data points were taken could be important in evaluating our method.

(e) We plan to continue to improve and evaluate the system.

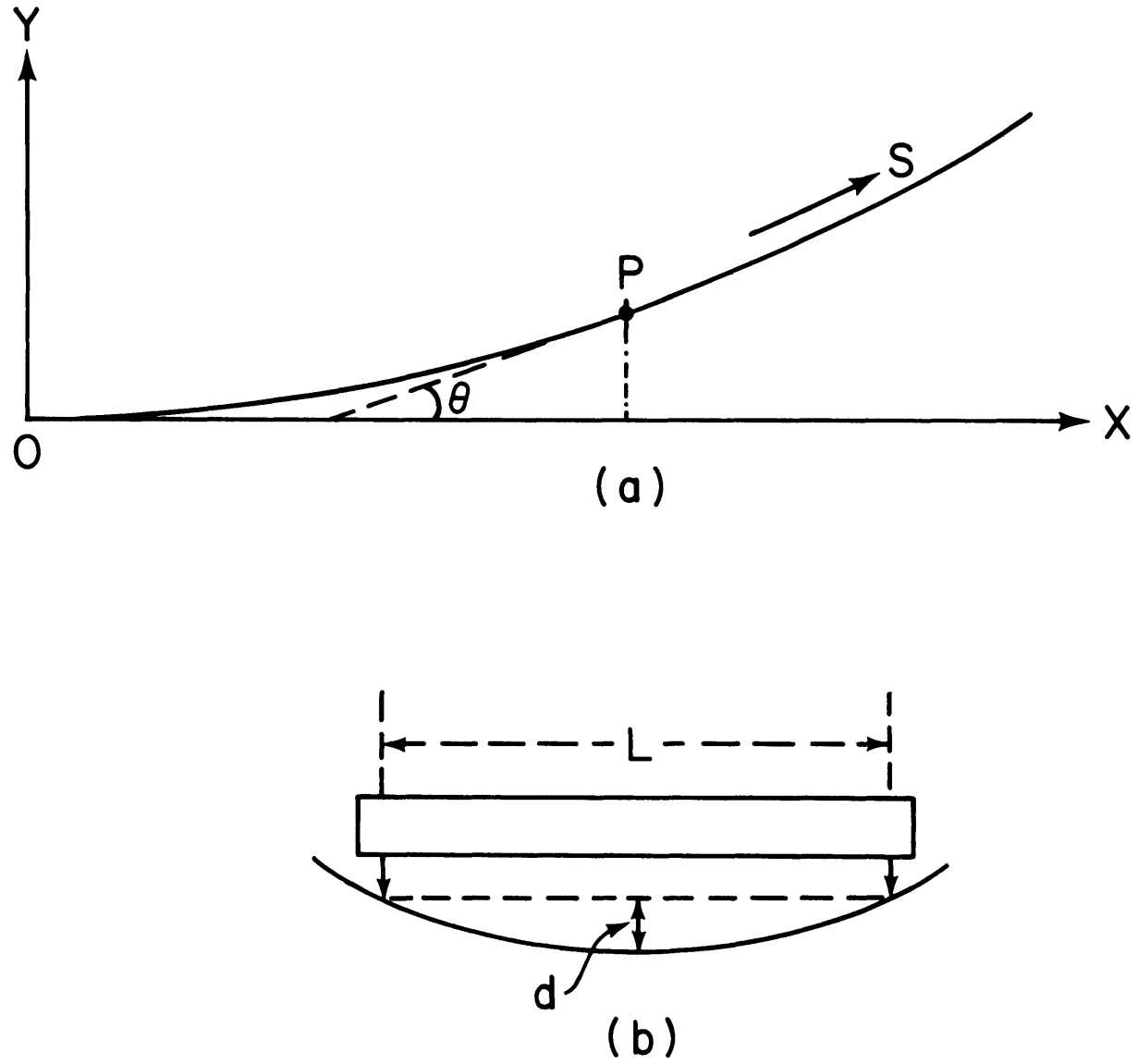

Figure III-16. The surface-measuring method. (a) Geometry of the surface. (b) Geometry of the measuring instrument.

APPENDIX II. SURFACE PLATES

The proposed surface plates for the 25-meter telescope are based on the plates designed for the 65-meter telescope. This includes building and testing five plates, two of which were manufactured by Philco-Ford and three by NRAO. The surface errors of these plates caused by manufacturing tolerances, gravitational deformation and temperature effects are summarized here. Based on these data, the surface errors of the 25-meter telescope are estimated.

Manufacturing Tolerance. The error derived from the inaccuracy of manufacturing is not firmly established. Studies have shown that for a reasonable cost surface plates of cast aluminum alloy milled by numerically controlled machines are promising. The numerically controlled machine is capable of working to within 13 μm of the data recorded on tape. Yet it was difficult to locate a manufacturer who was willing to accept a specification of manufacturing tolerance of 25 μm rms. Two test plates, manufactured by Philco-Ford in 1972 for the 65-meter telescope design study to a specified manufacturing tolerance of 64 μm rms, have been measured. The measured errors for these two plates are:

Plate 1 - 76 μm rms
Plate 2 - 41 μm rms

with an average of 59 μm. This figure is adopted as a realistic and conservative tolerance, assuming the plates are to be manufactured by this approach. However, the following points should be emphasized: (1) the required manufacturing accuracy for these two plates was only 64 μm, and (2) the capacity of the milling machine was not fully exploited.

The adjustable NRAO plates, made from off-the-shelf aluminum pieces, united to a rib system with 36 adjustment screws, achieved a manufacturing accuracy of 56 μm for a plate 1.8 m long. Since the bumpiness of the plate changes with respect to the size to the 1.5 power, the manufacturing error estimated for the 1.5 m long plate is 40 μm.

Different approaches, such as grinding and polishing, would yield a smaller manufacturing error. The use of a servo-controlled milling machine instead of a directly controlled machine might improve the milling accuracy to 25 μm. For this reason, 25 μm is adopted as an "optimistic" manufacturing tolerance. Cost estimate of this approach will be available soon.

Thus the present manufacturing tolerance is assumed to be 59 μm, the planned tolerance 40 μm, and the future plate may be as good as 25 μm.

Gravitation deformation. The estimate of this error contribution is relatively simple. This can be achieved either by analytical approach with a computer model, or by direct measurement of a prototype. The measured result on the plate of length 1.8 m shows a gravitation deformation of 35 μm rms. The gravitational deformation of plates of similar design are proportional to the square of its size. The gravitational deformation of a 1.5 m plate will then be 24 μm rms. Since this deformation is measured under the worst case conditions (plates horizontal), a factor of 0.5 is applied to estimate the average gravitational surface error contribution when the telescope is tilted through its range of elevation motion. This gives a gravitational contribution of 12 μm rms.

Temperature deformation. A difference in temperature between the top surface and the bottom rib will introduce a surface error. For similar design, with identical temperature difference, the degradation of surface accuracy is proportional to the size of the plates. Measurements of the 1.8 m NRAO plate shows a temperature degradation of 41 μm/°C. This scales to a 38 μm/°C error for the 1.5 m plate proposed for the 25 m telescope.

APPENDIX III. DYNAMIC ANALYSIS

The telescope structure is massive and elastic, hence it can vibrate in a wide variety of oscillatory modes at various natural frequencies. It is important to understand these oscillations for two reasons:

(i) The dynamic behavior must be taken into account in the design of the drive and servo systems to ensure accurate tracking; (ii) the dynamic behavior must be compatible with the survival of all steel members under the effects of external driving forces such as wind. The latter reason may still apply to the 25-meter telescope inside a radome, if the radome takes the form of an astrodome.

The dynamic analysis must identify particularly two types of oscillation: (i) Those at the lowest natural frequency which generally involve the entire structure. This is because wind turbulence excites mainly low frequencies. For structures of the 25 meter size, theory and experiment show that energy exchange from the wind to the structure begins to fall rapidly in importance above 0.3 Hz. (For safety, the structure should have natural modes above $\sim$ 1.5 Hz.) (ii) Those of individual members, which may occur at high frequencies, are usually weakly coupled to the total structure. They must be assessed in terms of the survivability of the members involved.

The problem was analyzed in two separate stages. First, the reflector structure was analyzed. The reflector, feed legs, and elevation wheel, including the applied masses of the surface, were analyzed to determine the dynamic characteristics as seen by the elevation bearings. The elevation wheel is held at its lowest point, the model assuming infinitely stiff elevation bearings and drive points. This lumped-mass, spring model has 339 degrees of freedom, each with a particular stiffness. The dynamic behavior of the reflector, particularly the frequency of the rotational mode above the elevation axis, is of central importance in the design of the servo system for the elevation drive.

The dynamic equivalent of the reflector structure was next applied to the tower, and an analysis was made of the tower stiffness and inertia when supporting the corresponding spring-rates and masses of the reflector. Only the six lowest resonant frequencies of the reflector were analyzed. The tower itself is rendered as a lumped-mass spring model with 15 degrees of freedom. The dynamic behavior of the tower, particularly the frequency of the rotational mode about the azimuth axis, is important in the design of the servo system for the azimuth drive.

The following table lists the natural frequencies of the lowest oscillatory modes of the 25-meter telescope in the preliminary design.

Table III.4

Major Oscillatory Modes for the 25-meter Telescope

Component	Mode	Frequency (Hz)
Reflector structure	Rotational mode about the elevation axis	6.7
	Rotational mode about the azimuth axis	7.7
	Up and down mode in direction of azimuth axis	8.4
Tower structure	Side sway in direction parallel to elevation axis	7.6
	Side sway in direction perpendicular to elevation axis	11.7
	Rotational mode about the azimuth axis	11.9

All individual structural members were found to have natural modes and stiffness compatible with survival in a 120 mph wind. (Higher wind velocities were not analyzed.)

APPENDIX IV. SURFACE ERRORS DUE TO 30 km/h WIND

Wind on the parabolic surface of the radio telescope distorts the structure, causing a reduction of aperture efficiency of the telescope. The degradations of the telescope performance by wind are the result of the following effects:

1. The perturbing force distorts the backup structure, panel structure and surface plates, increasing the surface roughness.

2. The defocussing effect due to the distortion of the backup structure.

The wind forces and the response of the telescope varies, depending upon such properties of the structure as the f/D ratio, the porosity of the surface, the mounting configuration of the dish, etc. Wind tunnel tests conducted by various institutions on different antennas produce slightly different results. The test results by Jet Propulsion Laboratory of Pasadena were adopted for this investigation. Based on these test data, it is possible to predict the surface and pointing errors at various antenna positions. In this preliminary study, however, only the worst conditions for force (which is face on) were analyzed, and a factor of 1/3 was employed to illustrate the telescope's average performance over the whole sky.

The wind effect on the 25-meter antenna was not investigated during this preliminary study. However, extensive work was done in the area on the 65-meter antenna design. Since these two antennas are similar in design, it is possible to scale from the wind deformation of the 65-meter antenna with reasonably correct results. If the 25-meter design is a scaled-down design of the 65-meter design in geometry only, with all cross-sectional areas of the members remaining unchanged, then the scale factor for the wind deformation is the third power of the dimensional ratio. On the other hand, if the cross-sectional area of the members were also reduced according to the scale, then the scale factor for the wind deformation is only the second power of the dimensional ratio. In the case of

the 25-meter design, the reduction of cross-sectional area of the members does not fall on these two limits, but lies somewhere in between. For the reason of being conservative, the second power was adopted. It should be emphasized that it is possible to reduce the wind deformation by stiffening up the structural design, if there is a change of the basic philosophy that the structure is not protected by an enclosure.

The following table gives results for wind on various components of the telescope. The dimensional ratio for the backup structure and the subreflector is 25/65, for the panel design 1/2, and for the surface plates 60/75.

Table III.5

The Effect of 30 km/h Wind on the Surface Errors

Source of Error	rms error (μm)
Effect of wind on the backup structure, including equivalent error due to reflector defocussing	11
Effect of wind deforming the panel structure	5
Effect of wind deforming the surface plates	10
Effect of wind on subreflector support, including tilting and lateral transition--translated to equivalent surface error	1
Total error (rss)	16

APPENDIX V. A COMPUTER CONTROLLED SURFACE ADJUSTMENT DEVICE

Introduction

The 25-meter telescope requires a setting of surface plates to an accuracy of 15 μm rms. With such a requirement and the vast number of adjustment screws (2112 screws with 0.5 hr per screw for manual operation), the effort required is estimated to be 0.5 man-years. In order to reduce the setting time, a semi-automatic setting device, driven by motor and controlled by computer, is being developed. The estimated time for the setting of the surface plates is then 3 man-months.

This device will also reduce the possibility of human errors. The on-line computer contains in its memory the amount of adjustment for each screw, defined by the best-fitting process. A binary code, encoded permanently on each setting assembly, triggers the computation while the motorized setting wrench is manually connected to the setting screw, resolving the amount of adjustment required on the screw. This amount will be converted into pulses through an interface, driving the stepping motor in a finite amount of rotation and a specified direction. The stepping motor in turn drives the wrench while connecting the setting screw. It is expected that the final setting accuracy of the surface plates will be improved.

Requirements on the Surface Plates

It is desirable to have this setting device well-developed prior to the manufacture of surface plates. Tentatively the plate manufacturer should provide four holes at each corner of the plate. The diameter is about 60 mm. The center-line alignment of each hole is perpendicular to a plane, defined by reference points on each plate. The alignment should be kept within 18 arc sec to this plane. The holes should be securely covered by a flat lid, threaded around the rim, so that the adjustment assembly could be covered all the time during the telescope operation.

The Setting Screw Assembly

Figure 1 shows the assembly with items described as follows:

(1) One-half inch diameter rod, with 20 threads per inch in unified thread series and a 3A classification.

(2) Three half-inch hexagon heavy jam nuts.

(3) Two washers, spherical on one side with a radius of 1.5 inches and with a hole of 0.6 inch in diameter.

(4) Mono-ball assembly with special nut insert (3/4 inch).

(5) Filler, linking between the setting assembly and the surface plate and holding the mono-ball in place. A unique screw I.D. in binary is encoded on the filler.

(6) Three guide rails, arranged in an unsymmetrical way to insure a one-way insertion. This will prohibit the operator from standing on the plate while adjusting. It also will insure the binary code mates with the receptacle during insertion.

(7) Upper template block to fill the upper portion of the screw during installation, holding the 1/2-inch rod perpendicular to the plane of the surface plate.

(8) Lower template block to be placed between the surface plate and the backup panel structure during installation to insure all plates are set approximately at the same height, prior to the preliminary setting.

(9) Flat, circular lid to keep the setting screw covered when the telescope is in operation.

Motorized Setting Wrench

Figure 2 shows the design with items described as follows:

(1) Stepping motor with 1°.8 per step, 200 steps per revolution (SLO-SYN model M061).

(2) Steel spur gear reducers with pitch diameters of 1" and 5", forming a planatory two-stages of 5:1 gear reduction.

(3) One-half inch lock nut wrench (maximum 0.510", min. 0.504") driven by a 3/8" torque wrench (New Britain TW-35, 100-ft/lb capacity).

(4) Three-fourths inch setting nut wrench (max. 0.763", min. 0.755") connected to the 5" gear.

(5) Wrench housing to house the setting nut and locking nut wrenches. It also provides the mating configuration to the guide rail to insure one-way insertion. A 12-bit switch for the binary code is located at the tip of the housing in order to transmit the information of screw identification.

(6) Two solid bronze cylinder bearings.

Translator

Translator receives pulses supplied by a computer and converts the pulses into the switching sequence needed to drive the motor in steps. The translator will drive the motor one step for each pulse received. It has the logic capacities for bi-directional stepping control.

Interface

A communication link between the computer and the translator. It converts the digital output of the computer into pulses. It also receives commands from the computer and converts it into a control to the direction switch in the translator.

Computer

The on-line computer proposed for the telescope is adequate for this purpose. Software is in development.

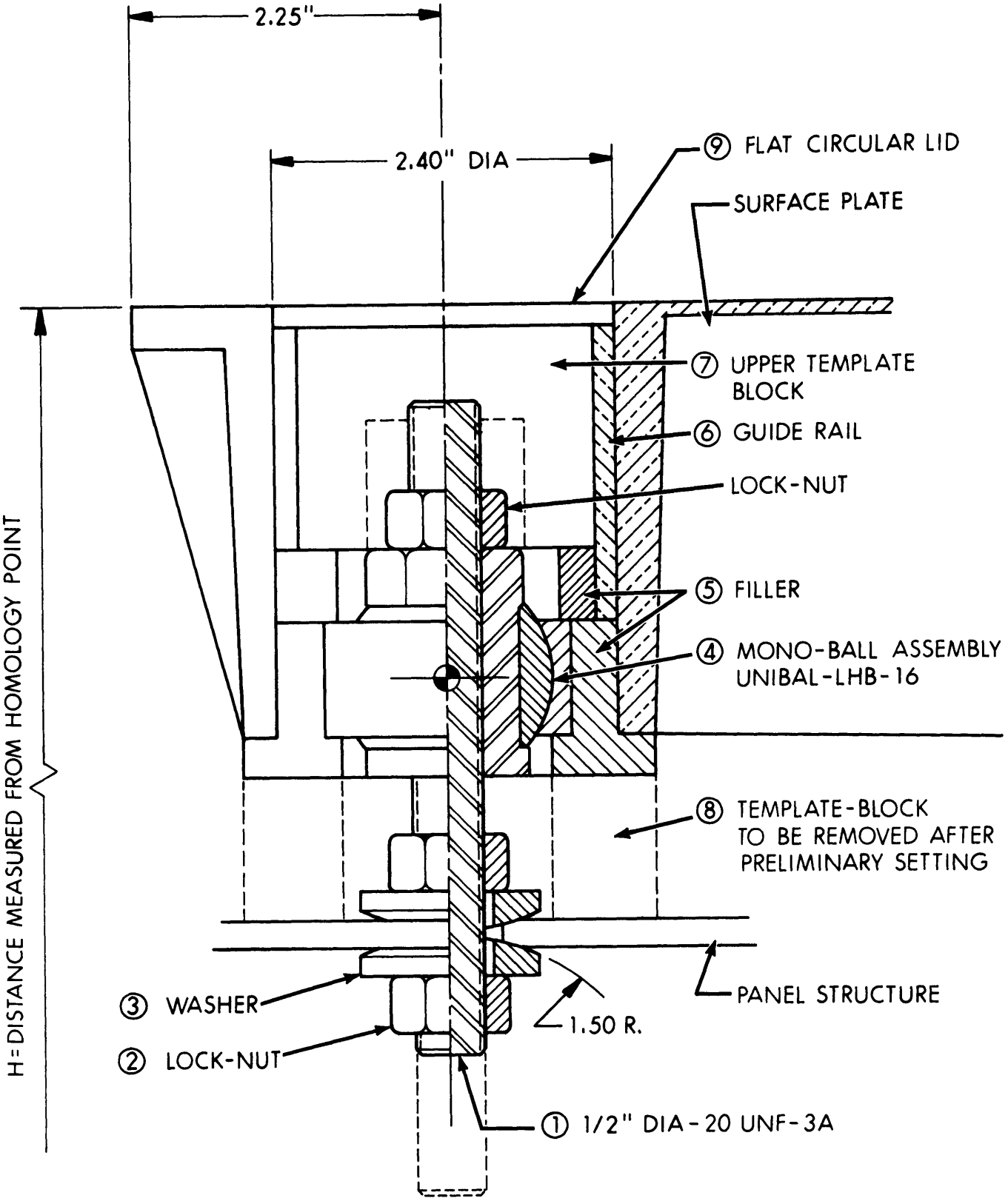

Figure III-17. Setting screw assembly.

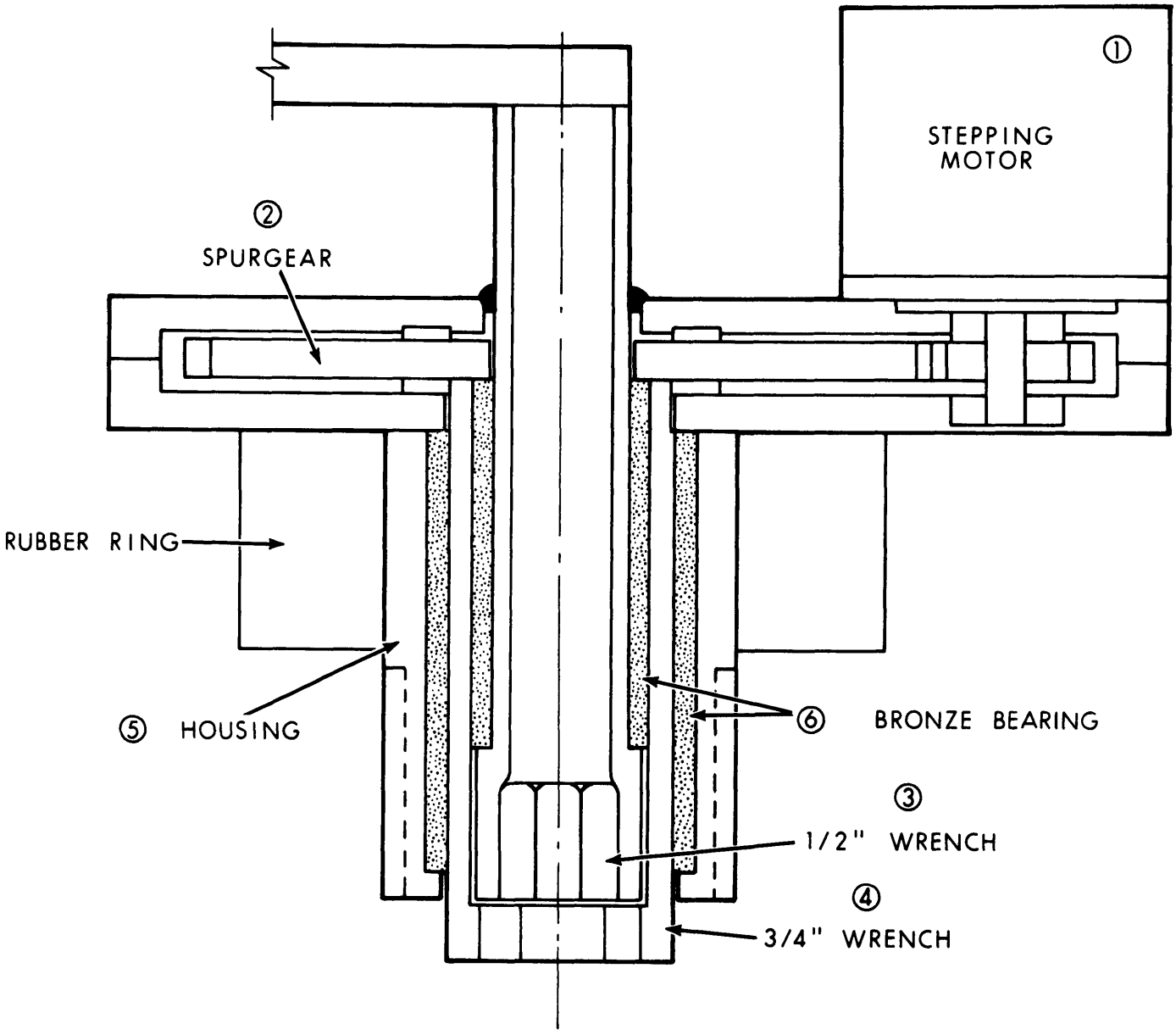

Figure III-18. Motorized setting wrench.

APPENDIX VI. SUMMARY OF ENGINEERING DATA AND RELATED INFORMATION FOR THE 25-METER DIAMETER RADIO TELESCOPE

Weight

Component	lbs.	Sub-total lbs.
Feed leg structure	2,200	
Panels	39,000	
Surface plates	22,213	
Loading at feed	2,000	
Loading at vertex	2,000	
Backup structure	64,600	
Counterweight	30,000	162,000
Tower	82,400	
Elevation bearings (2)	1,000	
Elevation drive (2)	4,000	
Azimuth drive (8)	8,000	95,400
Azimuth trucks (4)	48,000	48,000

Total weight on elevation bearings = 162,000 x 1.1

= 178,000 lbs.

= 89 tons

Total weight on azimuth truck and pintle bearing = (162,000 + 95,400) x 1.1

= 283,000 lbs

= 141.5 tons

Total weight above the azimuth track = (162,000 + 95,400 + 48,000) x 1.1

= 335,940 lbs.

= 168 tons

Optics	
Diameter	25 m
Focal length	10.5 m
f/D	0.42
Magnification	15.8
Effective focal length	166 m
Aperture Blockage	
Feed leg structure	6.4%
Gaps between plates	0.2%
Antenna Performance	
Required	
Total surface error	$\lambda/16$ = 75 μm
Shortest equivalent wavelength (η = 32%)	1.2 mm
Pointing accuracy	1.2 arcsec
Half-power beamwidth	12.1 arcsec
Mass Moments of Inertia	
Elevation structure about elevation axis	12.95×10^9 lb-in^2
Entire instrument about az axis	42.22×10^9 lb-in^2
Dynamics	
Acceleration and deceleration rate	0.25°/sec^2
Slew rate - elevation	20°/min
Slew rate - azimuth	40°/min
Travel range - elevation	0° to 125°
Travel range - azimuth	$\pm$ 270°

Lowest Natural Frequency

Elevation structure, with respect to the elevation axis	6.7 Hz
Entire instrument, with respect to the azimuth axis	11.9 Hz

Azimuth Drive System

Axis	Azimuth Axis	Gear Output Pinion	Gear Input Pinion
Gear ratio	1	30	10350
Gear ratio		1	345
I - Antenna	42.22×10^9 lb.in.^{2}	46.91×10^6 lb.in.^{2}	394.13 lb.in.^{2}
I - Gear boxes (8)	50.83×10^9 lb.in.^{2}	56.48×10^6 lb.in.^{2}	474.52 lb.in.^{2}
I - Motors (8)	34.54×10^9 lb.in.^{2}	38.37×10^6 lb.in.^{2}	322.40 lb.in.^{2}
Total moment of inertia	12.76×10^{10} lb.in.^{2}	141.76×10^6 lb.in.^{2}	1191.50 lb.in.^{2}
Inertia torque at 0.25°/sec^2	12.00×10^4 ft.lb.	4000.00 ft.lb.	11.594 lb.in.^{2}
Gear box friction torque at 40°/min	4.34×10^4 ft.lb.	1446.24 ft.lb.	4.192 ft.lb.
6 mph wind torque	0.97×10^4 ft.lb.	323.32 ft.lb.	0.937 ft.lb.
Pintle bearing friction torque	0.03×10^4 ft.lb.	9.00 ft.lb.	0.026 ft.lb.
Drag of cable wrap	-	negligible	-
Total torque required	17.34×10^4 ft.lb.	5778.6 ft.lb.	16.749 ft.lb.
Max. speed	1/9 rpm	3.33 rpm	1150 rpm

Elevation Drive System

	At Elevation Axis	At Output Pinion	At Input Pinion
Gear ratio	1	75	20700
Gear ratio		1	276
Moment of inertia - antenna	12.95×10^9 lb.in.^{2}	2.30×10^6 lb.in.^{2}	30.2 lb.in.^{2}
Moment of inertia - gear box (1 of 2)	39.71×10^9 lb.in.^{2}	7.06×10^6 lb.in.^{2}	92.7 lb.in.^{2}
Moment of inertia - motor (1 of 2)	17.27×10^9 lb.in.^{2}	3.07×10^6 lb.in.^{2}	40.3 lb.in.^{2}
Moment of inertia - total	129.91×10^9 lb.in.^{2}	22.56×10^6 lb.in.^{2}	296.2 lb.in.^{2}
Max. gear box friction	13563 ft.lb.	180.8 ft. lb.	0.65 ft. lb.
Max. torque due to air circulation	7944 ft. lb.	105.9 ft. lb.	0.384 ft.lb.
Max. bearing friction during tracking	108 ft. lb.	1.4 ft. lb.	0.005 ft.lb.
Max. acceleration torque during slew	122,230 ft. lb.	1630.0 ft. lb.	5.905 ft.lb.
Total torque required	143.845 ft. lb.	1918 ft. lb.	6.949 ft.lb.
Max. speed	1/18 rpm	4.17 rpm	1150 rpm

Gear Box

Type	Philadelphia 7HP4 (modified)
Weight	440 lbs/box
Number required	2 for elevation axis; 8 for azimuth axis
Static efficiency	90%
Dynamic efficiency	93%
Rated torque at output pinion	31000 lb.in.
Stiffness at output pinion	1.5×10^6 ft.lb./rad.

Motor

Type	H.K. Porter Model #DFT4K7708
Speed	1150 rpm

CHAPTER IV

RADOMES

A. THE DESIRABILITY OF A RADOME

A spaceframe structure or radome offers substantial advantages for the 25-meter telescope in three areas: (i) it decreases the effects of thermal deformation in the structure; (ii) it shields against wind-induced deformations and pointing errors; and (iii) it provides a controlled environment for more reliable operations and for ease of maintenance of both the telescope and the radiometers. A radome has been required in some cases to ensure the survival of the telescope under extreme conditions of wind and ice. However, this is not important for the 25-meter telescope, which is designed to survive winds of 120 mph without protection.

The advantages of the radome must however be weighed against the following undesirable features: (i) there will be loss of signal arising from the geometric blockage by the radome structure and from the transmission loss in the radome fabric; (ii) the performance of the telescope is further degraded when the radome is wet, and may be degraded with time as the enclosure fabric "weathers" because of wind-blown dust or solar ultraviolet radiation; and (iii) there might be a limit set to the sensitivity achievable in beam-switched continuum observations since the two beams look through slightly different parts of the enclosure.

1. Radome Losses

Radome losses arise from blockage by the metal spaceframe members and from transmission loss through the radome fabric.

The blockage by the spaceframe members--the aperture obscuration--is the orthographic projection of the members on the antenna aperture, weighted by the aperture illumination function. A well-designed spaceframe will have blockage of approximately 10%. This loss is independent of frequency for wavelengths small compared with the size of the structural members.

The transmission loss in the radome fabric is mainly due to reflection; the maximum loss is determined in large part by the dielectric constant of the material, and the behavior as a function of wavelength is dependent on the thickness of the material. There will be no difficulty in finding a material whose maximum loss below 300 GHz is 20%, and there is at least one material whose loss is only 15%. We shall take therefore 25% as the total loss introduced by the radome. The loss can be reduced substantially below this at selected wavelengths by proper design of the radome and its fabric.

For purposes of comparison with losses due to deformation in the telescope, it is noted that a telescope having a surface accuracy of 75 μm inside a radome introducing a loss of 25% is equivalent in sensitivity at 1.2 mm to a telescope outside the radome with a surface accuracy of 91 μm. Alternatively, the integration time to achieve a given sensitivity is a factor of 1.8 greater for the telescope in a radome compared with the same system outside the radome.

2. Temperature Induced Errors in the Telescope Structure

In Chapter III it was shown that under sunlit conditions with no wind the exposed telescope will have thermal gradients across the structure which lead to pointing errors and a loss of efficiency. The rms pointing error under full sunlight can be as much as 6.3 arcsec (Table III.1), rendering the dish unusable at 1.2 mm and reducing the efficiency at 2 mm by approximately one-half. The degradation of the surface and backup structure is also severe. Again from Table III.1, assuming direct sunlight with no wind, the surface accuracy will decrease to 337 μm, rendering the dish unusable below 3.5 mm; the exposed dish would be competitive with the undisturbed dish in a radome only for wavelengths longer than 7.7 mm.

In order to estimate the fraction of the day during which temperature gradients of a given magnitude might be expected, the data from von Hoerner (1971) will be used. These data, taken for 27 days in Green Bank, give values

of the ambient temperature, the rate of change of that temperature, and the temperature differential between the skin and the ribs of a test surface plate, all as a function of the time of day. It might be expected that the temperature differentials at higher altitudes will be greater than these values, since the transmissivity of the atmosphere is greater (the transmissivity at 0.5 μm is 0.76 at 2700 feet, and 0.84 at 14,000 feet).

The average measured value of the temperature difference in the plate is used, without correction for the angle of illumination, since this will be more representative of a typical observing condition. Thus, using the thermal coefficients calculated in Chapter III, it is found that for a sunny day in which the cloud cover is less than 40% the rms of the surface exceeds the radome equivalent (91 μm) for 11 hours, and exceeds 110 μm (aperture efficiency at 1.2 mm of 16%, half that of the undistorted telescope) for 8 hours. The thermal effects are obviously much reduced on cloudy days, although temperature differences of up to 2° C (corresponding to a surface rms of 135 μm) were measured on days that had cloud cover of 80%.

The thermal effects will be dependent on the detailed climatology of the site selected for the instrument. As an example, we will use Mauna Kea. Statistics on the amount of cloud cover during the day are unhappily very sparse. It is known that three-quarters of the nights are suitable for photometry or spectroscopy. Approximately three-quarters of the mornings are clear or with scattered cloud (cover less than 50%) during which an exposed telescope would develop large thermal gradients. Most afternoons are overcast, during which the telescope would begin to stabilize, but will undergo distortion again towards sunset when the temperature changes rapidly and the clouds subside to lower altitudes. It appears therefore that in spite of the afternoon clouds the telescope will suffer thermal deformation during the daylight hours on three-quarters

of all days. As an estimate of the magnitude of the effect we will adopt the figures above, i.e., 11 hours with the rms greater than 91 μm, 8 hours with the rms greater than 110 μm.

3. The Effect of Wind-Induced Errors

In contrast to the temperature deformations, the wind-induced errors primarily affect the pointing of the telescope, rather than the surface accuracy. For example, Table III.1 shows that a wind of 30 km/h actually improves the surface accuracy somewhat, because it reduces the thermal differentials. However, the rms pointing error increases from 1.2 to 3.2 arcsecs, equivalent to reducing the efficiency from 32% to 21%.

In some programs, such as point source detection experiments, the equivalent sensitivity loss is the principal effect. For this type of observation, the net loss induced by wind equals the radome loss at 1.2 mm for winds greater than 28 km/h. The telescope will be unusable at 1.2 mm (equivalent aperture efficiency less than 15%) for winds greater than 34 km/h. However, for those observations in which maps of radio sources are desired the rms pointing error must not exceed 10% of the full beam-width (i.e., 1.2 arcsec at 1.2 mm). Otherwise, a serious loss of resolving power occurs, and it cannot be recovered by further observations.

As might be expected, the distribution of night wind speeds is strongly dependent on the site, and again we will use Mauna Kea as an example. Data for one year (Morrison, et al. 1973) show that the wind exceeds 25 km/h approximately 25% of the nights, during which the losses are equivalent to those imposed by the radome, and exceeds 33 km/h on 20% of the nights, during which it is unusable at 1.2 mm.

It is of course possible to stiffen the present design to lessen the wind-induced pointing errors. It will require further detailed design to see if it is possible to reduce the error by the required factor of three. Stiffening the telescope will require more steel, although perhaps not as much as for a spaceframe, and it will not significantly reduce the thermal errors.

4. Other Aspects of Radomes

Although the effects of the metal spaceframe and the dielectric cover are the most important, there are a number of others which must at least be mentioned. These have been discussed in the context of radio astronomy by Meeks and Ruze (1971), following a series of measurements on the Haystack antenna.

(i) Radome noise contribution: The radome contributes noise due to reflections from the spaceframe and the radome cover, and from emission from the cover. At 22 GHz the total is approximately 20 K for the present system. With a better spaceframe and cover this quantity could be kept to about 20 K at 100 GHz and 35 K at 300 GHz; these are small compared with anticipated system temperatures.

(ii) Gain and noise granularity: Measurement on the Haystack antenna have shown that the change of gain between directions a few beamwidths (up to about one-half degree) is less than 0.25%, and that the fluctuation in background temperature is less than 0.1 K. These quantities can be reduced by a factor of two with an improved spaceframe. The change in gain is acceptably small, but if the noise granularity is close to 0.1 K it might limit continuum observations of sources of angular scale comparable with the spaceframe member length (on Haystack, 1.5 degrees of arc). Beams switched over a few minutes of arc should see much smaller differences.

(iii) Polarization effects: No polarization effects were found on the Haystack antenna at 8 GHz to a level of 0.2%. The polarization effects should be absent at much shorter wavelengths.

(iv) The effect of rain: During periods of rain the system temperature will increase, by perhaps 100 K, and the signal will suffer increased attentuation. However observations will be curtailed during rain in any event, and if the radome can be treated to enhance drying, the recovery time after rain might be reduced to as little as one hour.

(v) A controlled environment for operations: Since the telescope is not exposed, the operation of it and its electronics will be more reliable, and maintenance will be easier.

5. Summary

Within the accuracy of the crude estimates made in the preceding sections, there is no clear advantage to using a radome in terms of observing time. Without the radome approximately two-thirds of all daylight hours will be lost due to thermal effects, and between 20 and 25% of the nights will be lost because of wind. In contrast the telescope in the radome will operate under all conditions, but will require integration times approximately 1.8 times longer to make up the radome loss. However, considering that the thermal effects may be greater on a high mountain top and that the radome losses may be reduced below the values assumed, and in view of the considerable advantages to the operations that a radome provides, we conclude that the 25-meter telescope should be placed in a radome.

B. RADOME FABRICS

In the preceding section it was assumed that the transmission loss in the radome fabric would not exceed 15% at frequencies as high as 300 GHz. Several new types of fabrics have recently been developed which appear to offer much higher transmission at these frequencies than previous radome fabrics. Some of the new materials are still proprietary to industrial firms, but their general properties have been obtained through the firms or through tests conducted on samples at the NRAO.

The transmission loss in the radome fabric is a function of the wavelength, the dielectric constant and loss tangent of the material, the thickness of the material, and the angle of incidence of the radiation. However, for all materials that might be considered, the resistive loss is small compared to the reflective loss over the wavelength range of interest. The effect of oblique incidence of the radiation will be similar

for most of the materials. The principal criterion for choosing amongst the various materials will therefore be the maximum reflective loss up to 300 GHz. It is important to note that if the electrical thickness of the material is a multiple of a half-wavelength, the loss will be much less than the maximum.

Griffolyn is a polyethylene-base fabric whose transmission for wavelengths up to 300 GHz is calculated to be at least 80%, based on the measured loss at 55 GHz of a sample 0.1 mm thick, and assuming that the losses at higher frequencies do not involve lattice modes. Experience with other polyethylenes suggests that these transmissions may well apply up to 1000 GHz (300 μm). The durability of Griffolyn under harsh weathering conditions has not been fully tested, and polyethylenes in general are degraded by ultraviolet radiation. However, tests of samples at Green Bank over an eight-month period show no visible signs of degradation. Griffolyn appears to have adequate tensile strength for radome use. A 3 sq. ft. sample 0.1 mm thick was found in tests at Green Bank to withstand the equivalent of 500 km/h wind loading without rupture, although it lost some elasticity at only 100 km/h equivalent wind. A sample 0.2 mm thick starts to lose elasticity at 200 km/h equivalent wind, and has 20% loss of transmission up to about 300 GHz.

The cost of Griffolyn is very low, about 5 cents per sq. ft. for material 0.1 mm in thickness. The cost will increase somewhat less than linearly with thickness.

Schjeldahl (a material designated G1249 from G T. Schjeldahl Co.) is a somewhat stronger but less flexible material than Griffolyn. It consists of four layers: tedlar/mylar/mylar/dacron, the tedlar layer providing weather-proofing and the dacron layer providing strength. Our test sample was 0.3 mm thick. It measured 8.4% loss at 60 GHz, increasing more or less monotonically to 30% loss at 300 GHz (by calculation). These losses are rather higher than we consider desirable. G1249 appears to be highly durable against weathering, and sheds water well. No cost estimate

is available, although it is expected to be somewhere between the inexpensive Griffolyn and the expensive fabrics which ESSCO is studying.

ESSCO Corporation Fabrics. In cooperation with Dupont, the ESSCO Corporation has developed several materials which, in regard to transmission properties, appear to be the best available. One such material, designated X-99-2A, consists of a layer of highly transparent material (composition not divulged) surrounded on both sides by a layer of tedlar or other special weather-proof substance that sheds water well and is resistant to ultraviolet radiation. The three layers total 0.6 mm in thickness. Transmission measures made at the National Physical Laboratory, England, indicate losses of about 15% to 300 GHz and at most 20% to 700 GHz. Unfortunately, material X-99-2A is not sufficiently flexible to be used in a removable aperture covering such as described in Section IV.C. The cost of this material has not been definitely set, but probably will be between $20 and $50 per sq. ft. Another ESSCO material, designated X-10-15, measured 9.6% loss at 60 GHz and is expected to be only slightly inferior to X-99-2A at higher frequencies.

A considerably cheaper material is Esscolam-6, used by ESSCO Corporation in the mm-wave telescope radome for the University of Massachusetts. This material is 0.35 mm thick, has adequate strength and durability and costs $2 per sq. ft. Its transmission loss is 12% at 90 GHz, 22% at 150 GHz and 28% at 400 GHz.

Additional study is required before we can decide on the best material for our purposes. The long-term durability of all fabrics must be thoroughly assessed. The behavior of the fabric when contaminated by dust or grit must be studied, since if the transmission degrades significantly for this reason, it will be an important factor in the choice of the material. Tests must be conducted to determine

whether some fabrics transmit less near-infrared solar radiation than others. Such radiation must be minimized in order to minimize vertical temperature gradients inside the radome. Finally, a detailed design of the spaceframe and radome fabric must be undertaken to see if it is possible to have the wavelengths of maximum transmission coincident with the atmospheric windows.

C. TYPES OF RADOMES

1. A Spaceframe Enclosure

This type of structure is nearly spherical in shape, completely enclosed, and consists of a lattice of steel structural members covered with a suitably transmissive fabric. The cell shapes formed by the structural members may be random in shape, so as to avoid "resonances" in the transmission properties at certain wavelengths or certain telescope positions. As a structure it is well understood, it is easily built, and it is relatively inexpensive. Detailed design work will be required to optimize its transmission properties.

In order to insure adequate circulation of air, the diameter of the spaceframe should be approximately 120 ft.

2. Astrodomes

If the enclosure contains a "window" which is either highly transparent or which can be removed entirely if the weather conditions are favorable, then many of the problems described previously can be avoided. No such enclosure--an astrodome--of the size required has been yet designed. In order to avoid blockage of the antenna beam over the full range of elevation, the aperture must be of order 100 ft. by 90 ft. However, the potential advantages of the astrodome are so great that it is useful to consider the basic concepts.

Some increase in the transmission over that given by the spaceframe can probably be achieved by means of a highly transparent window. The

typical radome fabrics will require support across the aperture, in order to withstand high winds. The supporting members might be made of material with a high dielectric constant, such as dacron or fiberglass. Such material would be better than a steel spaceframe, except at wavelengths for which there is a geometric resonance; in the latter case the blockage would be comparable with that of the spaceframe. Additional design studies will be required to determine if the improvement is great enough to warrant the additional structure complexity.

The alternative type of astrodome has a window with a removable cover. The cover might slide up over the roof, as is the case with the 36-foot telescope at Kitt Peak. This design has the disadvantage that the fabric must be flexible, which restricts the choice of material, and that the aperture cover over the required large area is not structurally rigid. As a consequence the aperture cover might suffer deformation under wind which would distort the incident wavefront and cause transmission loss.

A more promising approach is to remove the aperture cover by means of a laterally sliding door. The symmetric structure in which the door consists of two sections moving in opposite directions (employed, for example, in most optical telescope domes) is unattractive, since the large steel supporting members along the inner edges of the two halves will produce considerable blockage when the aperture is closed. Instead, a preliminary design has been developed (Fig. IV-1) in which the door, a segment of a spaceframe, slides to one side. Figure IV-1 (a) is a top view, (b) is from the front, and (c) is from the side. The dashed lines indicate the door, in the open position. The structure will not deform under wind loading when in the closed position, although when closed the transmission will be comparable with that of the spaceframe. It is however somewhat cumbersome, and requires a large wheel and track azimuth drive.

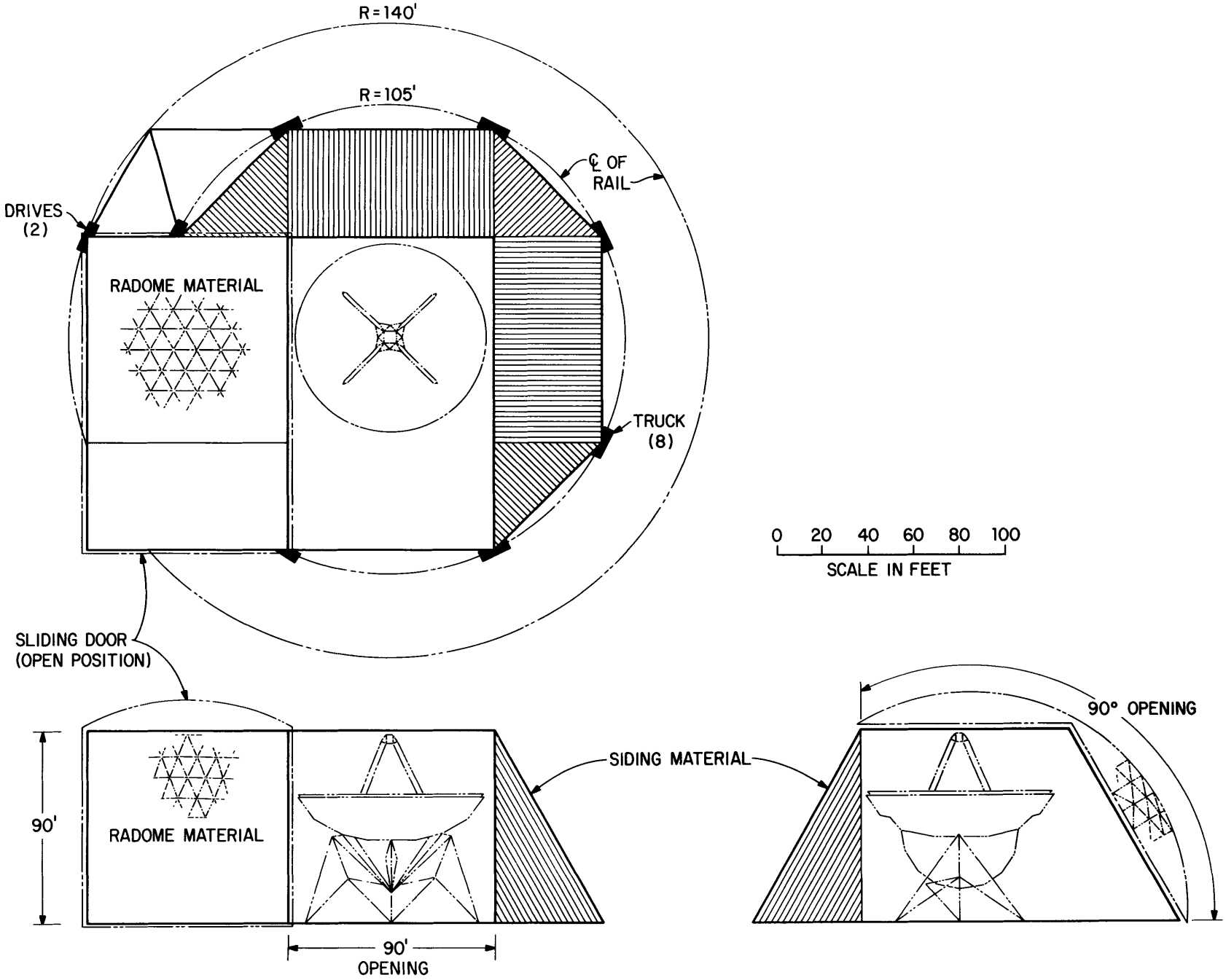

Figure IV-1. A preliminary design for an astrodome.
(a) Top view. (b) Front view. (c) Side view.

In summary, an astrodome for the 25-meter telescope is feasible, but more expensive than a spaceframe. It will require a much more detailed design effort to specify an optimum astrodome, and to determine if the increased performance of the telescope justifies the additional cost.

CHAPTER V

THE TELESCOPE SITE

A. BASIC CRITERIA FOR SITE SELECTION

The site chosen for the 25-meter telescope will have a significant influence on its ultimate performance. In the present section, we shall review in general terms the criteria which have guided our efforts to find a suitable site. Following sections will discuss atmospheric transparency and the specific sites which have been considered.

Atmospheric transparency is the most important consideration in siting a millimeter-wave telescope. The opacity of the atmosphere at millimeter wavelengths is both appreciable and variable. Obviously we require a site where the attenuation is low and stable for a major part of the time. Since most of the attenuation is caused by water vapor, which typically has a scale height of less than 2 km, this calls for a site at high elevation in an area where the local and large-scale climatic factors lead to generally dry air.

The instrument should be able to reach as much of the sky as possible. For this reason, it should be placed no farther from the equator than necessary.

The instrument can be used to its full potential only if it is adequately supported by a first-class resident operating and engineering staff. These people must be able to reach the instrument readily at any time; this is not a trivial problem when dealing with a high-altitude facility. It should not be appreciably more difficult to reach the instrument from its base laboratory than it is to reach the 11-meter telescope on Kitt Keak from the Tucson office. Moreover, living conditions in the vicinity of the site must be attractive enough to draw good personnel.

We have considered only sites in the United States, because of the practical difficulties of building, staffing and operating a facility

in another country. We have also restricted the search to sites which have at least minimal existing road access.

In summary, we require an easily accessible high-altitude site in a dry part of the United States, at low latitude, in an area where it is pleasant to live. The search has therefore been restricted to Hawaii and parts of the Southwest.

B. ATMOSPHERIC TRANSPARENCY AT MILLIMETER WAVELENGTHS

Figure V-1 (Findlay and von Hoerner 1972) shows approximately the spectrum of atmospheric absorption toward the zenith over the frequency range 1-500 GHz. Two curves are plotted, corresponding to 3.4 mm and 21 mm of precipitable water vapor (W_v) in the air path. Two sharp peaks due to oxygen (O_2) are constant and effectively saturated. The remaining peaks, and the general increase of absorption with decreasing wavelength, are caused by water vapor. Since the amount of water vapor varies with time, altitude, and geographic location, it is this quantity which must be minimized by an appropriate selection of the site.

Recent work by Wrixon (1973) shows that the zenith absorption A (in dB) is related to W_v (in mm) by

$$A = a + b\, W_v ,$$

where a is a constant and b depends on the frequency. Narrow-band observations, by Mather et al. (1971) and Wrixon (1973), scaled to an elevation of 12,000 feet, indicate that $a \approx 0.21$. The observations by Mather et al. give $b \approx 0.165$ at 230 GHz and $b \approx 0.95$ at 341 GHz. These frequencies correspond to atmospheric windows at the shortest wavelengths contemplated for the 25-meter telescope. The absorption is less, of course, in the windows at longer wavelengths.

It is not easy to assemble strictly comparable W_v data for all the sites of interest. Kuiper (1970) estimated W_v for a large number of locations from radiosonde data. Comparison of these values with later

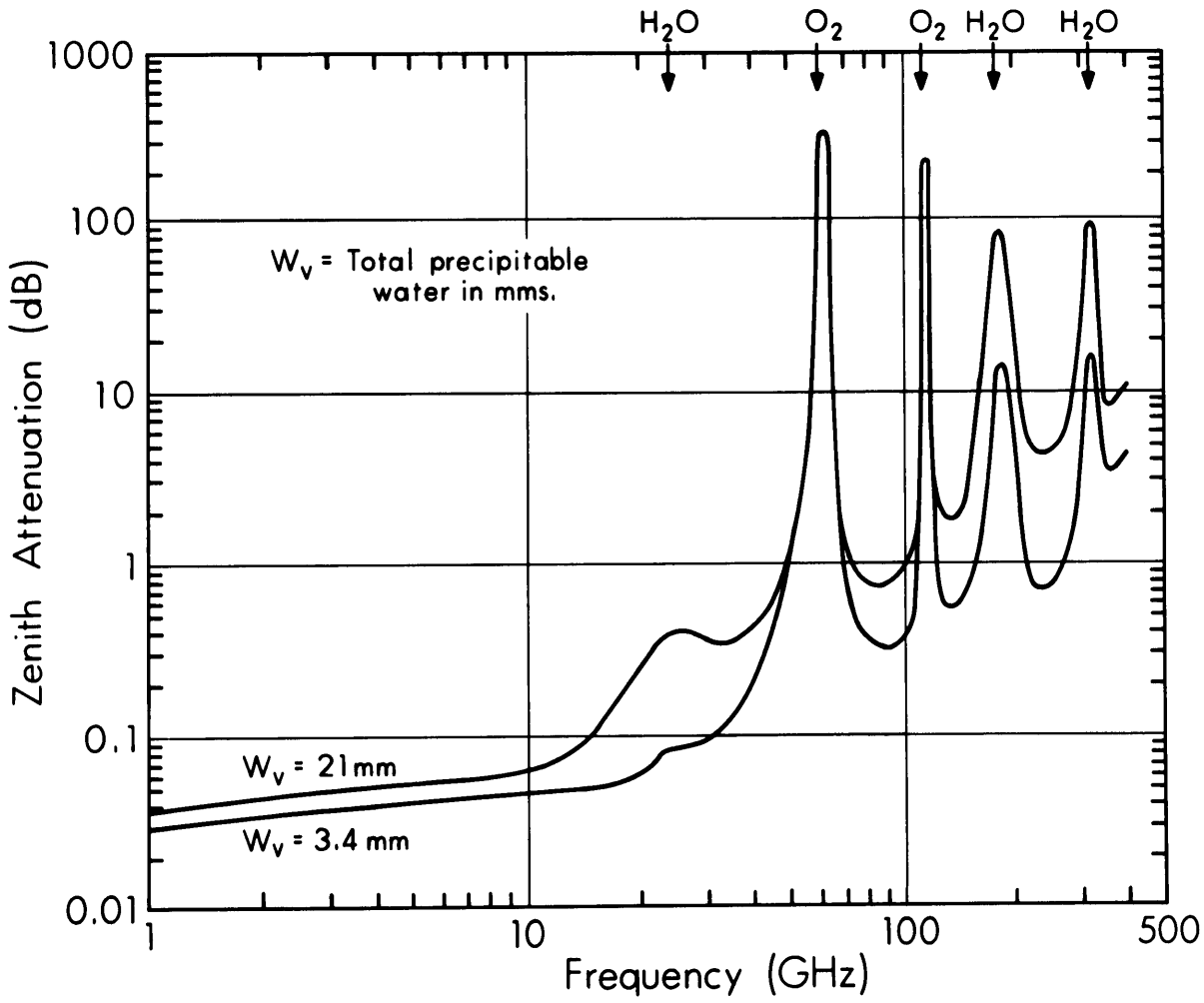

Figure V-1. One-way zenith absorption of radio waves in the atmosphere.

direct measurements shows that they tend to be too high. An important collection of direct measurements was made under the direction of Westphal (1974) during the search for a site for the National Infrared Telescope. These measurements were made during daylight on clear days with an infrared hygrometer over a one-year period. The Westphal survey included four of the eight sites considered for the 25-meter telescope. For the remaining sites, only estimates of W_v are available.

The values of W_v which are given in the next section refer to the 50^{th} percentile, i.e., the measured values were at least as low as the stated number half of the time. The Westphal figures require a correction for atmospheric pressure which has been incorporated in the quoted values. It must be remembered that all of these numbers refer to daytime in clear weather. Night values should be appreciably lower because of the substance of dry air from above.

The figures we give also refer only to the nine best months of the year. Sites in temperate latitudes become much wetter during the summer. There is little seasonal variation at the one tropical site (Mauna Kea).

C. SITES CONSIDERED FOR THE 25-METER TELESCOPE

Table V.1 lists the potential sites which have received serious consideration. The first two columns give the name of the mountain and the nearest city which could serve as a base for the facility. The third, fourth and fifth columns give the latitude, longitude, and elevation of the actual locations we have considered; these are not necessarily the summits of the mountains. The sixth column gives W_v for the best nine months of the year, in millimeters of precipitable water, for those sites included in the Westphal survey. The last column gives the estimated annual number of clear days (MacDonald 1958), defined as days with cloud cover less than 30% (the number of clear nights should be greater).

We turn now to a more detailed discussion of the sites listed in Table V.1.

Table V.1

Site	Nearest City	Latitude	Longitude	Elevation	W_v (mm)	Clear Days
Kitt Peak	Tucson, Arizona	31°58'N	111°36'W	6750 ft	3.3±0.8	260
Mauna Kea	Hilo, Hawaii	19°49'N	155°29'W	13630 ft	2.5±0.2	230
Mt. Epaulet	Denver, Colorado	39°34'N	105°38'W	13450 ft		160
Mt. Hopkins	Tucson, Arizona	31°41'N	110°53'W	8585 ft		240
Mt. Lemmon	Tucson, Arizona	32°26'N	110°47'W	9190 ft.	2.3±0.8	260
Pikes Peak	Colorado Springs, Colo.	38°50'N	105°02'W	13950 ft		160
South Baldy	Socorro, New Mexico	33°58'N	107°11'W	10800 ft		260
White Mountain	Bishop, California	37°37'N	118°14'W	13000 ft	1.5*±0.6	260

* Adjusted to 13000 ft, assuming water vapor scale height of 1.6 km.

1. Kitt Peak

This is the site of the Kitt Peak National Observatory and the NRAO 11-meter millimeter wave telescope. Although this site is attractive because of the easy access from Tucson and because it has excellent support facilities, work at the shortest wavelengths would be hampered seriously by the relatively low elevation and consequently higher W_v.

2. Mauna Kea

An extinct volcano on the island of Hawaii, Mauna Kea is the highest point in the Pacific. It is the site of the observatory of the Institute for Astronomy of the University of Hawaii. The National Infrared Telescope (3 m) will be built there, as will the United Kingdom Infrared Telescope (3.8 m) and the Canada-France-Hawaii Telescope (3.6 m). A 2.25 meter optical telescope and several smaller instruments have been in operation for several years. An excellent description of Mauna Kea as an observatory site has been published (Morrison et al. 1973).

The summit area is very dry. Most of the moisture remains below the tradewind inversion, which usually is near 8000 feet. Because of the extreme aridity, there is essentially no vegetation above 10,000 feet. According to Morrison et al., night-time values of W_v are frequently as low as 0.5 mm. Unlike the other sites in Table V.1, there is little seasonal variation of W_v.

The mean temperature is a few degrees above freezing. The diurnal and seasonal temperature ranges are 10° C and 6° C, respectively. Between sunset and sunrise, the temperature usually remains constant within 1° C. Winds are usually 10 to 15 miles per hour, although they are sometimes much higher.

The tradewind inversion usually breaks up late in the morning, and as a result there frequently is cloud over the summit in the afternoon. The rapid cooling at sunset generates strong downslope winds which carry the clouds and moist air down the mountain. Cool, dry air then remains over the summit until the next morning, when the cycle starts anew.

The location we have considered is Puu Poliahu, an isolated cinder cone about 1 km southwest of the summit. Seeing tests were made by Kuiper in the 1960's from this point. The road made for Kuiper is still usable.

The observatory is 60 km by road from Hilo, the principal city on the island. All but the last 10 km of the road is paved. The driving time from Hilo to the summit is 1.5 hours.

The astronomical environment, radio as well as optical, is well protected. There are few potentially serious sources of interference on the island. The University of Hawaii has a long-term lease from the State for the entire area above 12,000 feet, and the State and County governments are committed to preserving the astronomical quality of the site.

The University is building an office, dormitory, and dining complex on a 40-acre tract at the 8000 foot level, about 15 km by road from the summit. It is meant to serve all observers and institutions using Mauna Kea.

There are several direct flights from Los Angeles and San Francisco to Hilo each day (flying time four to five hours). There are numerous flights between Honolulu and Hilo.

3. Mount Evans/Mount Epaulet

Mount Evans is the site of a small infrared observatory operated by the University of Denver. Mount Epaulet is a shoulder of Mount Evans which offers a larger flat area for construction. The central office might be located in Denver (46 miles) or Idaho Springs (21 miles). Access to the summit during the winter would require the existing roads be improved.

There are no data on W_v for this site, but the value may be similar to that for Pikes Peak.

This site is probably inferior to Pikes Peak, which lies 50 miles to the south.

4. Mount Hopkins

This mountain is the site of a facility operated by the Smithsonian Astrophysical Observatory, and would also be served by a central office in Tucson. The only estimate of W_v is from psychrometric measures of surface absolute humidity, which indicate a value for the best nine months of 4.5 mm.

This site offers no apparent advantages over the nearby Kitt Peak and Mount Lemmon sites, while being much more difficult of access.

5. Mount Lemmon

This is the highest point in the Santa Catalina Mountains, an isolated range just north of Tucson. It is the site of the Mount Lemmon Infrared Observatory, which has several large instruments. It is managed by a consortium of the Universities of Arizona, Minnesota, and California at San Diego, and the Air Force Cambridge Research Laboratories.

The value of W_v is remarkably small, considering the relatively low elevation of the summit. Few other climatic data are available. The existing information suggests that the climate is generally mild, although considerable snow falls in the winter.

Mount Lemmon is approximately 60 km by paved road from the NRAO office in Tucson. Except for the final 3 km, snow removal is done by Pima County.

A serious concern with Mount Lemmon is the large number of radio transmitters. As of 1974, there were 89 within six miles of the site, ranging in frequency from 43 MHz to 11.38 GHz and in power from 4 W to 250 kW. Thus the radio-frequency environment is quite poor, and it would be very difficult to prevent further deterioration in the future because of the precedent which has been set.

6. Pikes Peak

Pikes Peak is a high, isolated mountain at the eastern edge of the Rockies. It is well-known as a tourist attraction, and it has an excellent road to the top. There are a restaurant (open in summer) and an Army physiological testing laboratory at the summit.

Pikes Peak is the cloudiest of the sites listed in Table V.1. The incidence of cloudiness ranges from 33% in November to 74% in July (Kuiper 1970). Recent work by Querfeld (1973) confirms that frequent cloud is a serious impediment to astronomical work on Pikes Peak. The value of W_v is 1.4 mm, marginally the lowest of the sites considered. This is not obtained from direct measurements, but from radiosonde data as analyzed by Kuiper. In other respects, the climate is not unfavorable (see Kuiper 1970).

The accessibility is very good, owing to the tourist road mentioned above. The driving time from Colorado Springs is about an hour and twenty minutes. During the winter, snow accumulates deeply on the road (which is not normally kept open between October and May). Snow removal is not difficult, however, and the road could be kept open through the year at moderate cost.

The most suitable location for the telescope would be the level shoulder just southeast of the summit. This has several acres of flat ground, is easily reached from the existing road, and is well removed from the press of tourists.

The summit area is managed by the City of Colorado Springs, under a long-term lease from the U.S. Forest Service. The City also maintains the road.

Although Pikes Peak is good in some respects, the high incidence of cloud makes is less desirable than other sites in Table V.1.

7. South Baldy

A 10,000 foot peak between the VLA site and Socorro, New Mexico, South Baldy is the location of the Langmuir Laboratory (for atmospheric studies) and the observatory of the New Mexico Institute of Mining and Technology. The site would be served by Socorro, and operations might benefit from the proximity to the VLA.

The W_v for the best nine months is estimated to be 2.4 mm, on the basis of hygrometer measurements made at lower elevations in the Plains of San Augustin.

Access to the site will be difficult unless the road is improved. In addition, there is potential interference from nearby radar used in the study of thunderstorms.

8. White Mountain

White Mountain is the highest point in the Inyo Mountains, the long range which forms the eastern boundary of the Owens Valley. The University of California has maintained research facilities on White Mountain for many years. Although the research has been concerned mainly with the physiological effects of high altitude, work has also been done in cosmic ray physics and infrared astronomy.

The air is extremely dry and the number of cloudless days is high. However, White Mountain has two disadvantages.

Occasional severe weather on White Mountain is one area of some concern. Winds can be higher than at other sites considered, exceeding 100 mph on occasion. Of more concern is the high incidence of precipitation from January through March, when the values of W_v are normally lowest. Fully one-third of observing time may be lost to precipitation during these months.

A second problem is the difficulty of access from Bishop, the only reasonable choice for a base city. The present road route is about 100 km long, requiring a minimum driving time of three hours. Parts of the last 40 km are closed by snow from November to May; snow clearance is probably not feasible because of continual drifting. We have not yet determined the cost of upgrading the road surface to reduce access time, and of fences to control snow drifting, but we expect the cost will be high.

Alternative means of access have been considered. The University of California uses a helicopter, but this is a poor solution since it is expensive, has a rather low payload, and is somewhat hazardous. Also the helicopter requires daylight and good weather. Another means of suitable access might be a tramway from the base of the mountain. It

is feasible but very expensive. Conservative estimates put the cost at $5 million for construction plus $250,000 annually for operation and maintenance. There may be an additional obstacle. Any possible route for the tramway must cross several miles of land now under consideration by the U.S. Forest Service for inclusion in the National Wilderness Preservation System. Final disposition of this land may not be made for several years.

D. SUMMARY AND CONCLUSIONS

Of the telescope sites discussed in the previous section, Mauna Kea appears to be the best possibility. Although other sites may have somewhat lower median W_v, Mauna Kea still has a sufficiently dry and stable atmosphere that should allow good observations at 1.2 mm much of the time and at 0.8 mm for some of the time.

Each of the other sites presents a particular difficulty. The Colorado sites are excessively cloudy and in addition have no direct W_v measurements. Kitt Peak and Mount Hopkins have high W_v, and the latter is more difficult of access. Mount Lemmon suffers from a poor radio environment. White Mountain has a difficult access problem and a severe winter climate. South Baldy is difficult of access and has a poor radio environment.

Mauna Kea is also favored by its low latitude, which makes more of the sky accessible to observation.

Finally, the fact that astronomical facilities already exist on Mauna Kea is a strong factor in its favor.

We conclude that of the several possible sites in the United States, Mauna Kea is most appropriate for the 25-meter telescope.

CHAPTER VI

COST ESTIMATES

A. SUMMARY

Estimated costs for the development, construction and operation of the 25-meter telescope are summarized in Table VI.1, and described in more detail later in this chapter. The estimates are in 1975 dollars. It is extremely difficult to estimate how costs may change in the next few years: If the average escalation is 10%/year, the cost in 1978 will be $12,276,000.

Table VI.1

Summary of Cost Estimates

Thousands of 1975 Dollars

Telescope		$ 2,873
Radome		2,805
Computer		476
Initial electronics		460
Site development		1,072
	Subtotal	$ 7,686
	20% contingency	1,537
	Total	$ 9,223
Operating cost -- $1,450/year		

The largest uncertainties in these estimates are in the cost of the surface plates and of the radome covering material. These represent about one-third the total cost and in both cases rather high estimates have been adopted. All other elements of the system are of conventional design and construction and cost estimates should be quite reliable. The 20% contingency should therefore be adequate.

B. FACILITY CONSTRUCTION AND DEVELOPMENT

1. The Telescope

Costs of various elements of the telescope are given in Table VI.2, with details described in the notes. Because the specific method of manufacturing the surface plates has not been selected, the highest of several estimates is used. Estimates for the structure are based on the detailed design described in Chapter III. Bearing and drive estimates are taken directly from the known costs of the VLA antennas.

2. The Control Computer

The computer system has been described in Chapter III, Section C-11. It is comprised of two minicomputers, one for telescope control and one for data processing, as well as the necessary digital interfaces, display and control devices, tape drives, and the disc memory.

3. Initial Electronics

Initial operation of the telescope will require feed systems, an LO system, a spectral-line backend, and a good front-end for the wavelength range 1.2 mm. Front-ends for other wavelength ranges will have been developed already for use with the 36 foot, and would be used (with repackaging) for this instrument. A continuing program of receiver development is envisioned as part of the operating costs.

4. Radome

A breakdown of the radome costs is shown in Table VI.3. The costs shown are for a standard spaceframe of diameter 120 feet, with radome fabric at $35 per square yard, typical of the more expensive fabric having lower loss. The cost of the radome could be reduced by $750K if the cheaper fabric is used, but at the expense of increasing the radome loss from 25% to between 30% and 35%. Since the better fabric is in an early stage of development, there could be a reduction in production prices.

No detailed cost is available for an astrodome, but it will cost more than the basic spaceframe-type of enclosure.

TABLE VI.2

Telescope Cost Estimates

	(Thousands of Dollars)
Surface plates	$ 753.0
Intermediate panels	275.9
Feed support	70.6
Subreflector	42.2
Backup structure	457.2
Counterweight	39.4
Bearings and drive	419.4
Servo	233.3
Tower structure	220.3
Foundation and track	216.5
Ladder and walkway	30.0
Cabling	50.0
Painting	65.0
Total	$2,872.8

NOTES TO TABLE VI.2

Surface Plates

Unit cost: $110/sq. ft.

Total surface area = 543 m^2 = 5,845 sq. ft. (Ref.: Chap. III)
Cost of surface plates 5,845 x $110/sq. ft. = $643K

Adjustment screws, material and installation	$110K
Total cost	$753K

Intermediate Structures

Total weight added 10%* = 39,000 lbs. x 1.1 = 42,900 lbs. (Ref.: Chap. III)

Material cost = 42,900 x 1.74 $/lbs. =	74.6K
Installation = 42,900 x 1.12 $/lbs. =	48.0K
Subtotal =	122.6K
Add 125% of engineering and burden =	153.3
Total =	275.9K

*Add 10% for all construction material due to waste.

Feed Support

Total weight added 10% = 2,200 lbs. x 1.1 = 2,420 lbs. (Ref.: Chap. III)

Material cost = 2,420 x 1.74 =	$ 4,211
Installation = 2,420 x 1.12 =	2,710
Subtotal =	6,921
Engineering and burden of 125% =	8,652
Total =	$15,573
Sterling mount =	55,000 (Ref.: 140 ft.)
Total cost =	$70,573

Subreflector

Scaled from the main reflector

Diameter of subreflector = 1.4 m (Fig. III.4)

Diameter of main reflector = 25 m

Total cost = 1.4/25 x $753

= $42.2K

Backup Structure

Total weight added 10% = 64,600 lbs. x 1.1 = 71,060 lbs. (Ref.: Chap. III)

Material Cost = 71,060 x 1.74	=	$123.6K
Installation = 71,060 x 1.12	=	79.6
Subtotal	=	203.2K
Engineering and burden (125%)	=	254.0
Total	=	$457.2K

Counterweight

Total weight added 10% = 30,000 x 1.1 = 33,000 lbs. (Ref.: Chap. III)

Material cost = 33,000 x 0.44 $/lbs.	=	$14,520
Installation = 33,000 x 0.09 $/lbs.	=	2,970
Subtotal	=	17,490
Engineering and burden (125%)	=	21,863
Total	=	$39,353

Bearing and Drive

All costs are in 1974 dollars.

Motors for both axes and two spares	$ 10,980
Brakes for both axes and two spares	4,200
Ten gear boxes and three spares	52,000
Azimuth truck units, four plus one spare	70,000
Elevation bearing	2,910
Pintle bearing	10,000
Cabling and hardware	8,000
Subtotal	$158,090
Total material cost @ 1974	158,090
Total material cost @ 1975 (assume 10%) =	$173,899

Estimated Engineering man-hour = 480 h @ $15/h

Estimated Labor man-hour = 480 h @ $11/h

Material cost	= $173.9K
Installation : Engineering	= 7.2
: Labor	= 5.3
Subtotal	= 186.4
Burden and Engineering (125%)	= 233.0
Total Cost	$419.4K

Servo

Position readout for two axes and one spare	$51.0K
D.C. amplifiers for both axes and two spares	18.1
Control panel and coarse readout	3.0
Miscellaneous electronics	5.0
Subtotal (1974 cost)	77.1K
Total material cost @ 1975 price (10% rate)	84.8K

Material cost		= $ 84.8K
Installation:	Engineering 320 h @ $15/h	= 4.8K
	Labor 1,280 h @ 11/h	= 14.1K
Subtotal		103.7
Burden and Engineering (125%)		= 129.6
Total cost		= $233.3K

Tower Structure

Total weight added 10% = 82,400 x 1.1 = 90,640 lbs.		
Material cost	= 90,640 x $0.72/lbs.	= $ 65.3K
Installation	= 90,640 x 0.36 $/lbs.	= 32.6K
Subtotal		= 97.9K
Engineering and Burden (125%)		= 122.4K
Total cost		$220.3K

Foundation and Track

Total volume of reinforced concrete = 310 c.y.		
Material cost = 310 x 137 $/c.y. =		$ 42,470
Installation = 310 x 96 $/c.y. =		29,760
Subtotal		72,230
Engineering and burden (125%) =		90,288
Total		$162,518

600-ft. 175 lbs. crane rail @ $40/L.F. including installation

Material and installation = 600 x 40 =	$24,000
Engineering and burden (125%) =	30,000
Total =	$54,000

Total cost = 162.5K + 54.0K = $216.5K

TABLE VI.3

Radome and Cost Estimate

	(Thousands of Dollars)
Space frame	$ 287.5
Covering material	1,400.0
Installation	147.2
Foundation	240.5
Service tower	61.0
Temperature control	688.5
Total	$ 2,804.7

NOTES TO TABLE VI.3

Radome

Surface area $\simeq$ 40,000 sq. ft.

ESSCO quote = Radome with $2/sq. ft. surface material would cost $330K; $10/sq. ft., $650K.

1974 price on the space frame = 330 -(40 x 2)= $250K

1975 price with 15% per annum = 250 x 1.15 = $287.5K

Use $287.5 for the cost of frame work

Material

$ 2/sq. ft. x 40,000 = $ 80K

$10/sq. ft. x 40,000 = $ 400K

$35/sq. ft. x 40,000 = $1,400K

NOTE: ESSCO standard material cost $10/sq. ft.

SCHJELDAHL cost less than $25/sq. ft.

But both of them has a loss more than 1 dB @ 200 $\sim$ 300 GHz

Only Griffolyn and X-99-2A are acceptable.

Cost of Griffolyn is $0.06/sq. ft.

X-99-2A is uncertain, ranged between

$10 $\sim$ $50/sq. ft. tentatively, use $35/sq. ft.

Installation: ESSCO @ 1974 = 128K

1975 @ 15% per annum = $147.2K

Radome

Service tower - 25 x 25 = 625 sq. ft. and 50 ft. high

Building cost = 625 x $40/sq. ft. = $25,000
Elevator (hydraulic) = 36,000
$61,000

Foundation for the radome diameter $\cong$ 150 ft
or circumference = 471 ft.
cross-section = 15 sq. ft.
volume $\cong$ 7,100 sq. ft. $\cong$ 262 c.y.

Material cost = 262 x $137/c.y. = $35,894
Installation = 262 x 96/c.y. = 25,152
T_1 = $61,046

For the floor disc with diameter $\cong$ 150', t = 0.5'.
volume $\cong$ 8,835 c.f. $\cong$ 327 c.y.

Material cost = 327 x $77.35/c.y. = $25,293
Installation = 327 x $62.80/c.y. = $20,536
T_2 = $45,829

$T_1 + T_2$ = $106.9K
Engineering and burden (125%) = 133.6K
Total $240.5K

Temperature control

Estimated capacity = 350 ton
Unit cost = 1,910 $/ton
Total cost = $668.5K

TABLE VI.4

Site Development Cost Estimates

	(Thousands of Dollars)
Road, water and sewer	$ 200.0
Power, standby generator	150.0
Control building (5000 ft^2)	275.0
Dormitory trailer	50.0
Utility building	60.0
Lab and office building (7500 ft^2)	337.5
Total	$1,072.5

NOTES TO TABLE VI.4

Site preparation

Water	$ 10,000
Sewer	20,000
Road	80,000
Electric	75,000
Grading	15,000
Total	$ 200,000

Stand-by generator - 500 KVA @ $300/KVA
= $150,000

Control building - 5000 sq. ft. @ $55/sq. ft.
= $275,000

Dormitory trailers - Use $50,000

Utility building - 200 sq. ft. @ $30/sq. ft.
= $60,000

Downtown building - 7500 sq. ft. @ $45/sq. ft.
= $337,500

5. Site Development

These estimates, detailed in Table VI.4, are preliminary estimates for a "typical" site and are not directly applicable to a specific site. In particular, the already existing and planned facilities on Mauna Kea might change the details considerably for that site. However, possible savings to be realized from pre-existing facilities may be offset by the somewhat higher construction and transportation costs of an Hawaiian site.

C. OPERATION

Table VI.5 shows the estimated annual operating costs.

Table VI.5

Operating Costs, in Thousands

Salary and benefits	$ 460
Material, services and supplies	790
Other observing equipment	200
Total (1975 dollars)	$1,450

The estimate is derived from our experience operating the Kitt Peak 36-foot telescope and the Green Bank facilities. It assumes an operating staff of 35 people.

REFERENCES

Findlay, J. W. and von Hoerner, S. 1972, "A 65-meter Telescope for Millimeter Wavelengths", NRAO, Charlottesville.

Kuiper, G. P. 1970, Comm. Lunar and Planetary Lab., 8, 121.

MacDonald, J. E. 1958, Univ. of Arizona. Inst. Atm. Phys., Sci. Rep. No. 7.

Mather, J. C., Werner, M. W. and Richards, P. L. 1971, Astrophys. J. Lett., 170, L59.

Meeks, M. L. and Ruze, J. 1971, IEEE Trans. Antennas Propagat., AP-19, 723.

Morrison, D., Murphy, R. E., Cruikshank, D. P., Sinton, W. M., and Martin, T. Z. 1973, P.A.S.P., 85, 225.

Payne, J. M., Hollis, J. M., and Findlay, J. W. 1975 (submitted to Review of Scientific Instruments).

Querfeld, C. W. 1973, "A Preliminary Report on the High Altitude Observatory Infrared Site Survey", NCAR Internal Report, Boulder.

von Hoerner, S. 1967, J. Struct. Div. Proc. Am. Soc. Civil Engrs., 93, 461.

von Hoerner, S. 1971, NRAO 65 m Telescope Report No. 36.

Westphal, J. A. 1974, "Final Report on the 10-Micron Sky Noise Survey", Calif. Inst. of Tech., Pasadena.

Wrixon, G. T. 1973, private communication.